Applying the Re-Os Isotope System to a Survey of Cratonic Bedrock in Northeastern Canada

Nadia Grisaru
Advisor: Alan Rooney
Second Reader: Noah Planavsky
April 29, 2019

A Senior Thesis presented to the faculty of the Department of Geology and Geophysics, Yale University, in partial fulfillment of the Bachelor's Degree.

Table of Contents

1. Abstract

Climate change, driven by anthropogenic emissions of greenhouse gases into the atmosphere, is proceeding at a rapid pace. Accurate climate models are essential in order to mitigate against rising sea levels, worsening draughts, and more frequent and more intense storms. Spatially and temporally distributed data is needed to refine these simulations. Current models rely heavily on studies of present-day systems and proxy data from the past 800,000 years. However, climates of the more distant past provide examples of environmental conditions that changed at rates comparable to those observed today. Understanding ice sheet behavior and collapse during intervals of elevated CO_2 concentrations is particularly important for predicting future sea level rise. This study seeks to contribute to the reconstruction of past ice sheet dynamics using proxy systems which enable the further refinement of climate models. The rhenium-osmium (Re-Os) radiogenic isotope system was used to analyze bedrock from Northeastern Canada, an area glaciated by the Laurentide Ice Sheet during the Pleistocene Epoch (2.5 – 0.012 Ma). This region was a major conduit for ice sheet discharge into the North Atlantic and Arctic oceans. The Os abundances and isotopic compositions and major and trace element data of 17 cratonic bedrock samples were measured. The Os isotope compositions of the samples vary widely ($^{187}Os/^{188}Os$ = <0.2 to >2.6), differing from typical continental crust values of ~1.4. Rocks with such compositions would be expected to upset steady-state marine conditions through contributions from glacial erosion and meltwater that were distinct from typical riverine inputs. This survey provides a basis for the comparison of North Atlantic marine sediment cores to continental bedrock source materials in order to better characterize the behavior of the Laurentide Ice Sheet during key transition periods.

2. Introduction

The climate is changing at a rate unprecedented in the history of the human species and the recent geological past. Paleoclimate records reveal that atmospheric temperatures and greenhouse gas concentrations exceed any on record in the last 800,000 years (Masson-Delmotte et al., 2013), and science indicates that humans are to blame. Anthropogenic emissions of gases like methane, CO_2, and nitrous oxide have risen exponentially since the beginning of the industrial revolution in the mid-1800s. Preindustrial levels of CO_2 in the late 18th century were

280 ppm; today they exceed 410 ppm (Masson-Delmotte et al., 2013). Once in the atmosphere, greenhouse gases absorb energy emitted by the Earth in the thermal infrared wavelengths (Marshall and Plumb, 2008). Some of this energy is radiated upward and eventually escapes into space, and a portion is radiated back down towards the planet surface. As a result, greenhouse gases cause a radiative forcing that effectively traps energy within the atmosphere, leading to increased global temperatures. For a greenhouse gas like CO_2, which has a residence time of several hundred years within the atmosphere, anthropogenic contributions outpace the depletion of the atmospheric reservoir (Marshall and Plumb, 2008). Concentrations build up, leading to warming.

In addition to grappling with the changes already underway, humans must plan for the future consequences of climate change. Climate models, built on mathematical equations based on laws of physics, fluid motion, and chemistry, generate forecasts which are essential to the formulation of appropriate adaptation strategies and climate policies (see Dutton et al., 2015 for a review). These models predict factors such as the intensity of major storm events, areas most susceptible to drought, and the rise in sea level over the next 100 to 1000 years. However, uncertainty due to a lack of understanding of *climate sensitivity* leads to variations between models, generating a range of forecasts (Dutton et al. 2015).

Rising sea levels have important implications for coastal cities and dwellers. Adaptation strategies rely heavily upon knowing the magnitude and rate of sea level rise, but this is difficult to quantify. Global warming causes large scale disruptions to ocean circulation and the hydrologic cycle through higher average surface temperatures and the increased flux of fresh water from land-based ice. Changes in ocean current patterns, thermal expansion, and glacier inputs can all impact sea level globally and locally (Masson-Delmotte et al., 2013). In the past hundred years, thermal expansion of the oceans and mass-reduction of alpine glaciers have been the most significant contributors to global mean sea level rise, but the Greenland and Antarctic Ice Sheets are both predicted to play a large role in the future (Dutton et al., 2015). An understanding of the geophysical dynamics of polar ice sheets is essential.

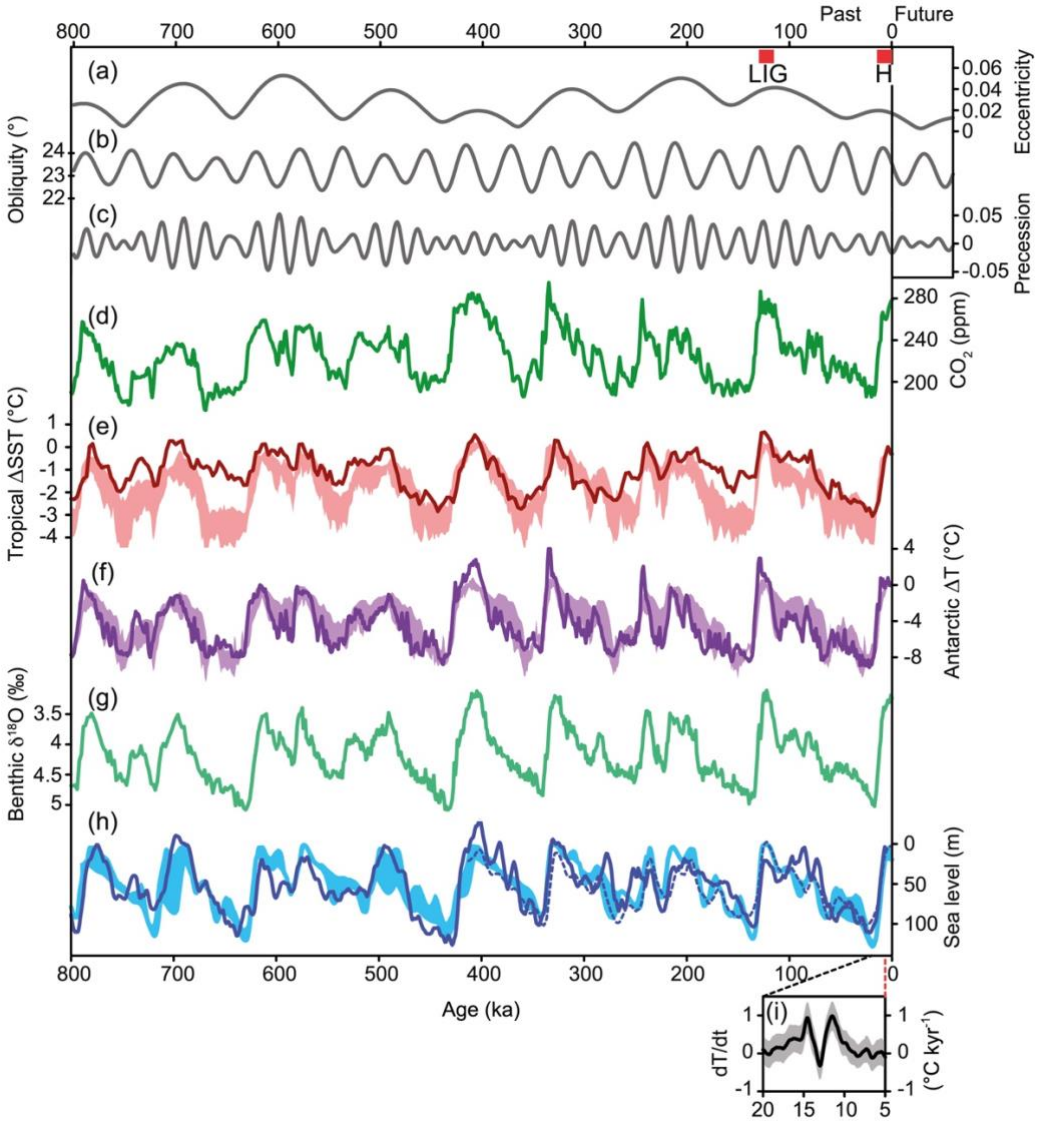

<u>Figure 1</u>: Orbital parameters and proxy records over the last 800 kyr. Oscillations in temperature, benthic $\delta_{18}O$, and sea level occur at 100 kyr periods (from Masson-Delmotte et al., 2013).

Current simulations of how ice sheets respond to a changing climate are based largely on the study of contemporary glaciers and the use of proxy systems like $\delta_{18}O$ (Figure 1). This data is used to refine and constrain models based on empirical observations. However, these proxies have considerable drawbacks such as salinity effects and complications related to ocean $\delta_{18}O$ signals responding to far-field ice-sheet behaviors that impact their ability to adequately inform the models. As Dutton et al. (2015), Raymo and Huybers (2008), and Cook et al. (2013) point out, drawing on data from past interglacial periods will further our understanding of how polar ice sheets respond to warming. Improving our knowledge of magnitudes, rates, and sources of

global mean sea level rise from polar ice sheet contributions requires a wide distribution of sea level reconstructions utilizing high temporal resolution data from sites near current and past ice sheets (Dutton et al., 2015).

This study seeks to contribute to the analysis of new proxy systems which would enable the further refinement of climate models. By compiling a geologic survey of bedrock from Northeastern Canada, an area of repeated past glaciations, this work provides a basis for future study of the dynamic behavior of Pleistocene ice sheets through the rhenium-osmium radiogenic isotope system.

3. Background

3.1. Pleistocene climate

The Pleistocene, the geological epoch from 2.5 – 0.012 Ma, was a time of increased and repeated continental glaciations (Raymo and Huybers, 2008). In addition to the ice sheets found on Greenland and Antarctica today, other large masses of glacial ice included the Laurentide and Cordilleran ice sheets on North America and the Fenno-Scandian ice sheet covering northern Europe. With more water stored in solid form as ice on land, sea levels around the globe were lower. Approximately 85% of the "extra" ice during this period was in the northern hemisphere (Roe, 2006). The Laurentide Ice Sheet (LIS), the focus of this particular study, covered much of what is today the northern Midwest and Northeast United States and eastern Canada, at times extending as far south as the 39th parallel (Balco & Rovey, 2010). The Hudson Straight, a channel linking the Atlantic Ocean and Labrador Sea to the Hudson Bay in Canada, was a major drainage conduit for the LIS. Evidence of interglacial ice sheet retreat and large melting episodes known as Heinrich events can be found in this area today, and calving ice bergs delivered subglacial debris to the North Atlantic Ocean where it is observed in marine sediment cores (Hemming, 2003). When the LIS began to disappear at the end of the Last Glacial Maximum (~20 ky BP) and ceased to exist entirely between 6,000 and 9,000 years ago, it contributed significantly to a rise in sea level (Ullman, 2016). By studying the glacial cycles of the LIS, a better understanding of ice sheet dynamics and sea level rise in response to widespread melting can be developed.

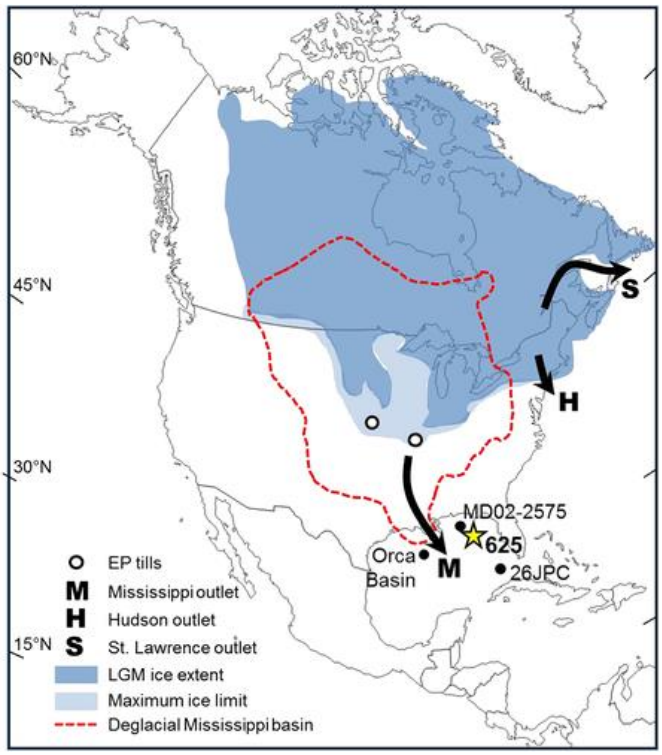

Figure 2: Average predicted LIS extents for the Last Glacial Maximum and the Pleistocene maximum (from Shakun et al., 2016). Arrows indicate drainage basins. The Hudson Straight drainage channel is indicated by the letter "S" and is the focus of this study.

Glacial periodicity is largely dependent on radiative forcing. In the 1920s, mathematician and geophysicist Milutin Milankovitch proposed a theory of planetary insolation to explain the effects of the Earth's movement on its climate. He argued that the periods of the variations in the Earth's orbit determine the planetary climate (Roe, 2006). Over large timescales, the orbit of the Earth around the sun changes ever so slightly. The orbital eccentricity – a measure of the elongation of the elliptical orbit of Earth – varies on 100 and 400 kyr periods, the orbital obliquity – the angle between the Earth's rotational axis and its orbital axis – varies on a 41 kyr period, and the climatic precession – how the seasons line up with Earth's revolution around the sun – varies on 19 and 23 kyr periods (Roe, 2006). As the orbit of the Earth is altered, insolation – the amount of radiation from the sun which reaches a given area of Earth over a period of time – changes. Milankovitch computed a time series of insolation as a function of latitude and season and used basic energy balance studies to estimate the resulting temperature changes (Roe, 2006). He noted that summertime insolation was a key factor in the mass balance of northern hemisphere ice sheets. These orbital cycles, he argued, helped determine the pace of Pleistocene ice ages.

For the early Pleistocene, Milankovitch's predictions are in-line with paleoclimate evidence. The 41 kyr observed glacial cycles were a result of the dominant effect of orbital obliquity on the climate system at the time (Clark, 2012). However, between 1.2 and 0.8 Ma, a shift, known as the Mid-Pleistocene Transition (MPT), from 41 to 100 kyr glacial periods occurred, apparently without any significant change in orbital forcing (Clark, 2012). The lack of change in outside forcing (e.g., orbital mechanics) suggests a more complex internal mechanism may underlie this change. A shift from low amplitude, high frequency cycles to high amplitude, low frequency can be observed in the deep sea $\delta_{18}O$ records (Clark and Pollard, 1998; Raymo and Lisiecki, 2004). The 100 kyr cycle maxima ice sheets were larger than their 41 kyr predecessors. Several models have been developed to interpret these observations. Explanations for the transition include ramping with frequency locking (RFL), a sudden increase in Antarctic ice volume, internal LIS dynamics coupled with changes in atmospheric CO_2 concentrations, and the regolith hypothesis (Nyman and Ditlevsen, 2019; Elderfield et al., 2012; Chalk et al., 2017; Clark and Pollard, 1998).

In simple terms, the Clark and Pollard (1998) regolith hypothesis postulates that a change from soft-bedded to mixed soft-hard bedded basal ice sheet conditions through the erosion and removal of a thick sediment regolith and the exposure of unweathered, crystalline bedrock resulted in thicker ice sheets with 100 kyr cycles and nonlinear deglaciation processes. Through the use of a one-dimensional model, Clark and Pollard showed how ice sheets scrape soft regolith to their margins through subglacial sediment deformation. This exposes hard, crystalline bedrock which provides more resistance to the ice sliding above it, resulting in slower glacial flow rates and the increased buildup of ice. The thin, extensive ice sheets associated with the early Pleistocene respond linearly to 23 and 41 kyr orbital forcing (Clark and Pollard, 1998). However, the thicker ice sheets after the transition exhibit 100 kyr cycles and nonlinear deglaciation processes due to the change in subglacial dynamics (Clark and Pollard, 1998). The model therefore agrees with the observed changes in glacial periodicity. This theory necessitates a confirmation of the change in basal conditions through paleoproxy data.

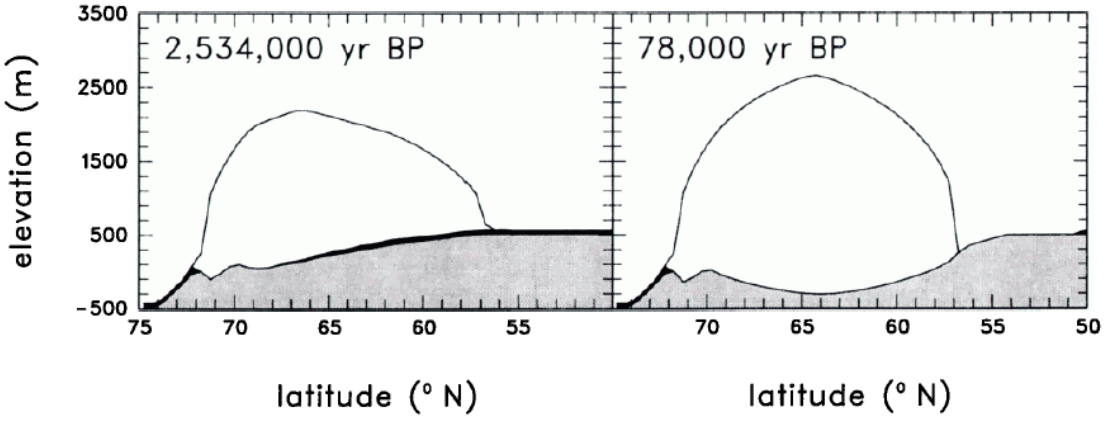

Figure 3: Clark and Pollard's (1998) ice sheet model. Right: before the MPT, Left: following the MPT. The regolith base (black) is scraped to the sides to expose the crystalline bedrock (gray).

3.2. Re-Os isotope geochemistry

The rhenium-osmium (Re-Os) radiogenic isotope system has recently been developed as a proxy for dating, determining past continental weathering, and reconstructing ice sheet behavior (Rooney et al., 2016). It is a unique system because Re and Os are siderophilic and chalcophilic, meaning they alloy readily with metallic iron and preferentially bond with sulfur over oxygen (Shirey and Walker, 1998). This marks a key difference from most other traditional long-lived radiogenic isotope systems which are lithophilic or oxygen-bonding (Shirey and Walker, 1998). As a result, Re and Os partition into metals or sulfides rather than silicates and can be found in rocks with elements that behave similarly (Stein and Hannah, 2014).

There are two naturally occurring isotopes of Re, stable ^{185}Re and radioactive ^{187}Re (Shirey and Walker, 1998). Os has seven isotopes: ^{184}Os, ^{186}Os, ^{187}Os, ^{188}Os, ^{189}Os, ^{190}Os, and ^{192}Os (Shirey and Walker, 1998). ^{186}Os and ^{187}Os are radiogenic and the latter isotope is derived from the β- decay of ^{187}Re (Shirey and Walker, 1998). The half-life of ^{187}Re is long, on the order of 41.2×10^9 years. (Stein and Hannah, 2014). However, the marine residence time of Os is sufficiently short to capture short-periodic fluctuations in continental weathering patterns, such as glacial-interglacial changes (Peucker-Ehrenbrink and Ravizza, 2000).

When measured in laboratory settings, abundances are normalized to ^{188}Os which is stable and has a fixed planetary abundance – converting and normalizing to isotope ratios removes the large uncertainties associated with measuring molar concentrations. Os is highly compatible in mantle sulfides and metal alloys, so it mostly stays in the mantle relative to the

crust (Shirey and Walker, 1998). Re, on the other hand, is only mildly compatible in the mantle, so it is much more readily transferred to the crust by partial melts (Shirey and Walker, 1998). The $^{187}Re/^{188}Os$ ratios of the crust are high and variable depending on the conditions and products of melt extraction. As ^{187}Re decays to ^{187}Os, the elemental abundance of radiogenic Os increases in the crust. As a result, older crust has a high ratio of $^{187}Os/^{188}Os$. Initial isotopic abundances of Os and sample ages can be calculated using the isochron equation (Stein and Hannah, 2014):

$$\left(\frac{^{187}Os}{^{188}Os}\right)_{measured} = \left(\frac{^{187}Os}{^{188}Os}\right)_{initial} + \left(\frac{^{187}Re}{^{188}Os}\right)_{initial} \left(e^{\lambda t} - 1\right)$$

Due to the long half-life of Re, 41.2 Gyr, the change in isotopic abundances in the last several million years is insignificant and present-day measurements can be used without correction. Rather than focus on these small changes, this study uses this isotope system to fingerprint and trace the continental origin of sediment in marine environments.

The Os isotopic composition of the oceans is a balance between unradiogenic sources and radiogenic sources (Figure 4). Hydrothermal processes at mid-ocean ridges, rain of cosmic dust, and the occasional meteorite contribute unradiogenic Os to marine environments (Peucker-Ehrenbrink and Ravizza, 2000). Radiogenic Os is added via continental weathering (Peucker-Ehrenbrink and Ravizza, 2000). Re and Os are redox sensitive. In oxic waters, Re and Os remain in solution where they are incorporated into organic matter (Peucker-Ehrenbrink and Ravizza, 2000). In sub-oxic to anoxic waters, the organic matter is preserved along with the Re and Os (Frank, 2002). Burial of organic matter under these conditions records the isotope composition of seawater at the time. The residence time of Re and Os in the ocean, ~780 kyr and <50 kyr respectively, is related to the input and output fluxes of the system (Peucker-Ehrenbrink and Ravizza, 2000). Marine residence times longer than the overturning circulation of the ocean result in well-mixed, homogenous isotope compositions except for in topologically restricted basins (Oxburgh et al., 2007).

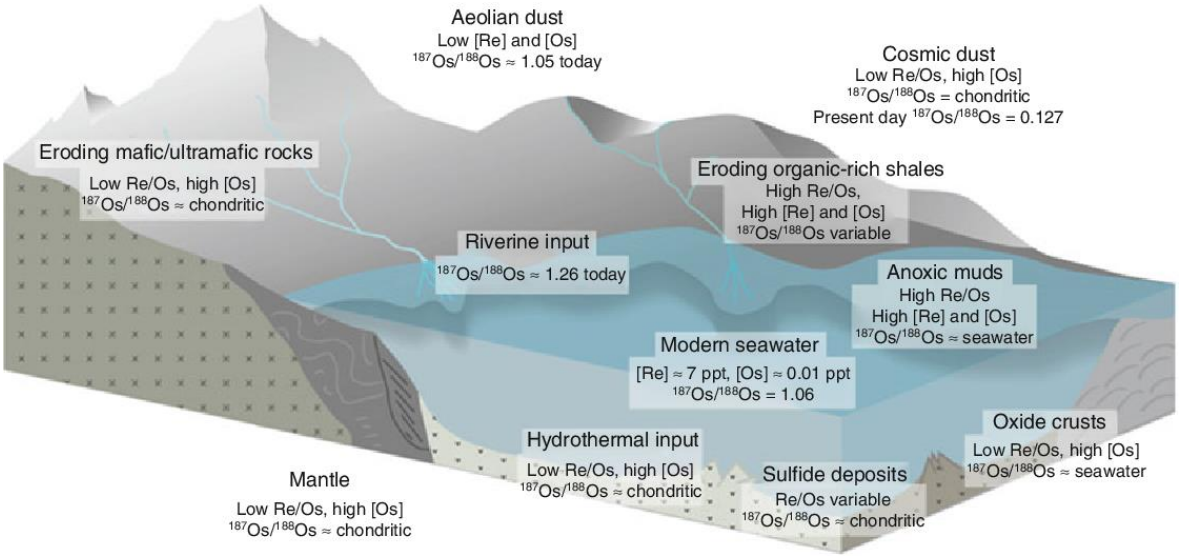

Figure 4: Re and Os reservoirs with sources and sinks for seawater (from Stein and Hannah, 2014). Concentrations of influx from continental weathering is highly dependent on the bedrock composition of the area. Average continental crust $^{187}Os/^{188}Os$ values are ~1.4.

In glaciated areas, Re and Os isotope compositions can be investigated by analyzing ice-rafted debris (IRD) buried in marine sediments. As glaciers scrape sediment and rocks from the subglacial surface, they become frozen into the basal ice (Hodell et al., 2008). In the case of marine-terminating glaciers, ice-bergs calve into the water and transport the glacial till frozen in their base out into the ocean (Hodell et al., 2008). As they melt, these rocks are dropped to the ocean floor and buried in sediments. These depositions are known as IRD. The quantity and type of IRD reveals information about the rate of ice flux into the ocean, the continental source of the icebergs, and ocean currents and temperature (Naafs et al., 2013). The isotopic composition reflects the source material. The IRD found in the northern Atlantic in marine sediment cores is thought to have originated primarily from the Laurentide Ice Sheet (Figure 5).

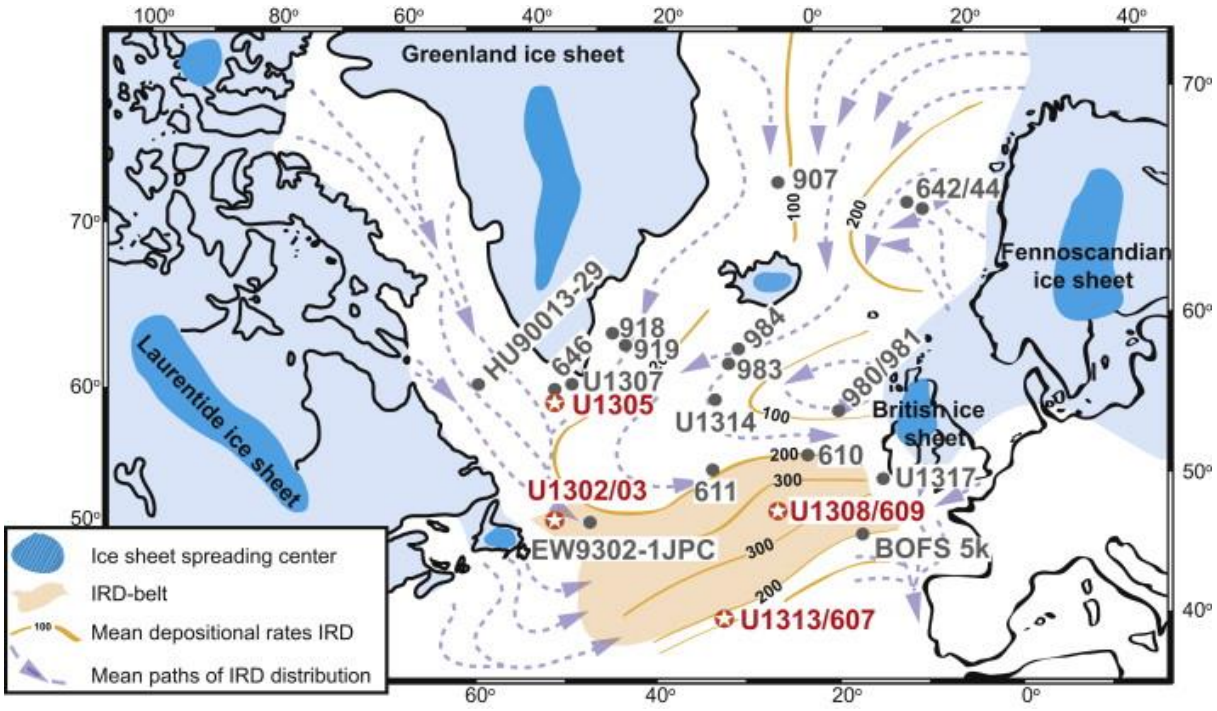

Figure 5: Average IRD depositional paths and sources for the North Atlantic (from Naafs et al., 2013). The IRD-belt, indicated in orange, corresponds to the last glacial period and likely varied for earlier glacial periods. Ice sheet centers are noted in blue, with the Laurentide Ice Sheet thought to have contributed the most to IRD-deposition in the North Atlantic. Marine sediment cores are indicated by the red stars.

Continental crust typically has a radiogenic Os isotopic composition of ~1.4 $^{187}Os/^{188}Os$ (Peucker-Ehrenbrink and Ravizza, 2000). Regolith, a heterogenous collection of unconsolidated rocky materials, has compositions in a similar range. Glacial erosion of continental sources with largescale deviations from this value can upset the steady-state marine isotopic compositions (Rooney et al., 2016). If Os from a large area of craton bedrock such the North American Craton in Northeastern Canada is deposited in ocean sediments via erosion, the subsequent isotopic variation can be traced back to its source. Deglaciation of the LIS, Heinrich events, or changes in subglacial conditions following the MPT are all expected to result in a deviation of bulk Os compositions in North Atlantic marine sediment cores at the strata concurrent with those erosional events.

The goal of this study is to create a geological and geochemical survey of the mineralogy, bulk Os concentration, and isotopic compositions of bedrock from the Hudson Straight area in Canada, the supposed origin of the IRD found in the North Atlantic Ocean. Seventeen rock samples were obtained from the Newfoundland and Labrador Province in eastern Canada and sent to Yale by David Corrigan (Geological Survey of Canada). Using Carius tube digestion and

negative thermal ionization mass spectrometry (N-TIMS), the bulk Re-Os abundances of the samples were determined. Thin sections and major and trace elements were assessed to ascertain the mineral composition of each sample in order to better understand the compatibility of Re and Os within the different types of source material from the area. In future work, the Re-Os composition of sediment cores from the north Atlantic containing IRD from the Laurentide Ice Sheet can be compared to the signatures of the continental source material analyzed in this study. If the Clark and Pollard regolith hypothesis (1998) is correct, a shift in isotopic composition is expected at the MPT – from earlier sediments reflecting a younger, less-radiogenic regolith origin to a later isotopic signal in line with the bedrock origins studied here.

4. Study Area

4.1. Geologic overview of the area

The Canadian Shield makes up the majority of the crust of eastern, central, and northwestern Canada ("Canadian Shield"). Continental shields – areas of low-lying, stable, Precambrian crystalline rock – are considered the nuclei of continental accretion ("Continental Shield"). The Canadian Shield is the largest mass of exposed Precambrian rock on the face of the Earth today, containing some of the oldest rocks in the world which are estimated to have been formed 4.28 Ga ("Canadian Shield"; "Tectonic Evolution"). Centered on the Hudson Bay, the shield is composed of four continents which coalesced between 2.0 and 1.8 Ga ("Tectonic Evolution"). Three of these masses acted as rigid cratons onto which further continental aggregation occurred. Their edges still bear evidence of folding and orogeny from more recent continental collisions and rifting events ("Canadian Shield").

The eastern edge of the Canadian Shield, spanning the province of Newfoundland and Labrador, is one such zone of border accretion (Figure 1). The Superior Craton, located inland to the west of the coast, provided a rigid, crystalline bedrock basement which remained stable throughout activity along the continental margins (Corrigan et al., 2016). It is bordered to the northeast by the Southeastern Churchill Province (SECP). Formed by the collision of the Superior and Nain (or North Atlantic) Cratons, the SECP contains two sections of younger formation age, the New Quebec and Torngat Orogens, and the Core Zone, an intervening block of Archean age (Wardle et al. 2011). Tectonic development of this area included the initial rifting of the Superior and Nain Cratons around 2.22 Ga, the collision of the Nain Craton and the

Core Zone to form the Torngat Orogen around 1.87 Ga, and the collision of the Superior Craton and the Core Zone to form the New Quebec Orogen around 1.82 Ga (Wardle et al. 2011).

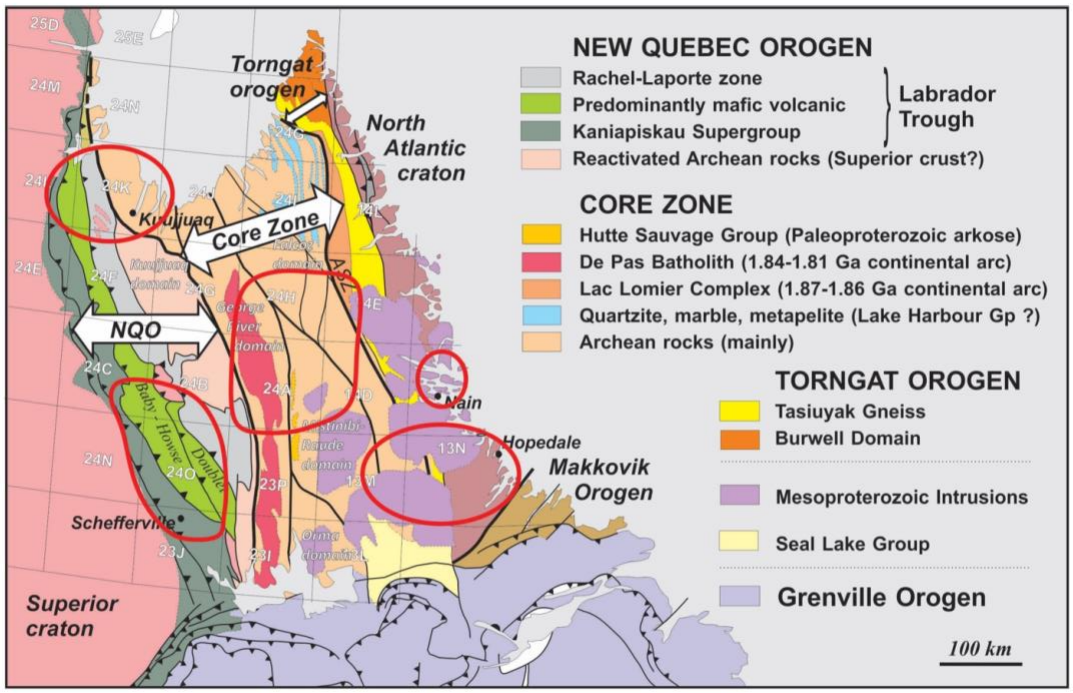

Figure 6: A geologic map of the Canadian Shield in the provinces of Québec and Labrador (from Corrigan et al., 2016). Zones of interest are outlined in red. The majority of the study samples were collected in these areas.

From west to east, the New Quebec Orogen, also known as the Labrador Trough, is a variably deformed and metamorphosed cover sequence with more deeply exhumed sections consisting of metamorphic plutonic rocks from the Archean and Proterozoic (Corrigan et al., 2016). The collision that resulted in the formation of the New Quebec Orogen is believed to have been relatively short lived with a dextral slip-strike component (Corrigan et al., 2016). To the east of the New Quebec Orogen, the Core Zone is composed of at least three lithotectonic entities (Corrigan et al., 2018). These distinct blocks, all Archean or early Proterozoic in age, consist of supracrustal rocks associated with intrusions, a volcanic arc with plutonic intrusions and clastic covering, and orthogneiss with intrusions (Corrigan et al. 2018). Similarly to the New

Quebec Orogen, the Torngat Orogen is the result of a doubly-vergent collision which resulted in metamorphic formations of variable grades (Corrigan et al., 2018).

4.2. Sample sites

Bedrock samples were collected by Dr. David Corrigan and the Geological Survey of Canada from sites in Newfoundland and Labrador over the course of 5 years. 17 samples were shipped to PhD student Erica Evans in Dr. Alan Rooney's lab for work in her graduate studies (Table 1). Samples were primarily collected from the North Atlantic Craton, Core Zone, and New Quebec Orogens. Rock types and dates, obtained from Dr. Corrigan along with the samples, indicate that the rocks are of igneous and metamorphic origins and are Archean or early Proterozoic, in line with current understandings of the geologic formation of these sites.

4.3. Rock types

Monzogranite (14CXA-D30c, 17CXA-D015)

A type of granite rock formed as the final fractionation product of magma. Monzogranites have high modal abundances of SiO_2, making them felsic. They are weakly peraluminous, containing slightly elevated ratio of Al_2O_3 to other major elements. They contain ilmenite, sphene, apatite, and zircon as accessory minerals (*Mindat*).

Megacrystic granite (14CXA-D072, 14CXA-D076)

A granite containing megacrysts, crystals or grains that are considerably larger than the matrix of the surrounding rock. Most likely formed earlier than the surrounding igneous rock as the lava cooled and hardened, crystal formation is partially dependent on temperature and pressure. Crystal composition can vary but likely is similar to the surrounding granite with high abundances of quartz and alkali feldspar (*Wikipedia*).

Tonalitic orthogneiss (14CXA-D097, 16CXA-D065, 17CXA-D018A1, 18CXA-D041)

Deformed and recrystallized tonalite. Percent composition of quartz and plagioclase feldspar are high, resulting in high abundances of silicon, calcium, and sodium (*Britannica*).

Gabbro (14CXA-D99)

A course-grained, dark-colored, intrusive igneous rock formed by the cooling and crystallization of molten magma under the surface. It is composed mainly of ferromagnesian minerals, especially pyroxene, and plagioclase feldspar. It is low in silicon (*Science Direct*).

Meta-siltstone (14CXA-D102)

A metamorphosed, sedimentary rock composed of >66% silt particles of varying origins. Formed in marine or lake basins, siltstones are primarily composed of quartz grains high in silicon and are associated with feldspar and mica flakes. Some siltstones also contain large amounts of carbonate (*Science Direct*).

Pillow basalt (15CXA-D002, 17CXA-D119)

A volcanic igneous rock that forms when basaltic lava erupts underwater and cools rapidly to form pillow shapes. Silicon abundances are relatively low, but basalts are magnesium and iron-rich, containing large amounts of calcic plagioclase feldspar and pyroxene (*Wikipedia*).

Psammo-pelite (15CXA-D005, 16CXA-D051)

A metamorphosed siltstone with a sandy component. Formed at the bottom of marine or lake depositional settings, silt grains are interspersed with larger sand grains. Both are high in quartz or feldspar abundances because they are the minerals most resistant to weathering (*Wikipedia*)

Grey quartzite (16CXA-D067)

A nonfoliated metamorphic rock that consists mostly of quartz. It forms during tectonic compression when sandstone with a high purity is heated under pressure. The sand grains melt and recrystallize. Quartzite comes in a range of colors but is usually white or gray. It is high in silica (*Thought Co*).

Anorthosite (17CXA-D001)

A phaneritic, intrusive igneous rock composed mostly of plagioclase feldspar, mainly anorthite, with a small mafic component. They tend to be calcium-rich with iron and magnesium as

secondaries. It is still largely unknown how anorthosites form, but the leading hypothesis is through the separation of plagioclase crystals based on their density (*Wikipedia*).

Tonalite/granodiorite (17CXA-D017)

Granodiorites are phaneritic igneous, intrusive rocks of felsic composition. Silicon percent abundance is high with quartz composing more than 20% of the rock. Plagioclase feldspar is present in large quantities with comparatively low abundances of orthoclase feldspar, resulting in more calcium and sodium and less potassium. Between 65 and 90% of the feldspar is plagioclase. Values at the high end designate the rock as tonalitic (*Wikipedia*).

Table 1: Site information for rock samples studied in this project. Samples were collected by Dr. David Corrigan and the Geological Survey of Canada and shipped to Erica Evans.

Sample Name	Rock Type	Age	Latitude (deg)	Longitude (deg)	Geological Province	Notes
14CXA-D30c	Monzogranite	ca. 1865 Ma	56° 53' 49" N	63° 19' 50" W	Lac Lomier Complex	part of ca. 1870-1860 Ma continental arc on North Atlantic Craton margin
14CXA-D072	Megacrystic granite	2322 ±5 Ma	56° 29' 00" N	64° 26' 28" W	Core Zone; Mistinibi-Raude Block	Representative plutonic rock; Pelland Intrusion
14CXA-D076	Megacrystic granite	ca. 1.83 Ga	56° 29' 51" N	65° 25' 00" W	Core Zone; De Pas Batholith	Representative sample from the middle of the batholith
14CXA-D097	Tonalitic orthogneiss	2856 ± 8 Ma	57° 03' 45" N	64° 39' 07" W	Core Zone, Falcoz Block	Migmatitic rock; sample is paleosome (non-melted portion)
14CXA-D99	Gabbro	1888 ±1 Ma	58° 29' 07" N	69° 35' 51" W	New Quebec Orogen; Montagnais Suite	Voluminous mafic intrusive suite; large proportion of Labrador Trough
14CXA-D102	Meta-siltstone	<2167 Ma	58° 29' 45" N	69° 37' 15" W	New Quebec Orogen; Labrador Trough	Marginal basin deposit, predates Montagnais sills
15CXA-D002	Pillow basalt	~1.88 Ga	58° 25' 40" N	69° 23' 31" W	New Quebec Orogen; Hellencourt Fm.	Voluminous basaltic suite
15CXA-D005	Psammo-pelite	<1.83 Ga	58° 23' 58" N	69° 06' 18" W	New Quebec Orogen; Rachel-Laporte Zone	
16CXA-D051	Psammo-pelite	<1.83 Ga	55° 47' 27" N	66° 32' 12" W	New Quebec Orogen; Rachel-Laporte Zone	Foreland basin with detrital source from the Core Zone

16CXA-D065	Migmatitic orthogneiss, tonalitic	~2.6 Ga	56° 07' 17" N	67° 13' 47" W	New Quebec Orogen; Wheeler Dome	uplifted basement, possibly linked to the Superior Craton
16CXA-D067	Grey quartzite	<2167 Ma	55° 07' 15" N	67° 29' 22" W	New Quebec Orogan; Kaniapiskau supergroup	meta-sandstone derived from erosion of Superior Craton
17CXA-D001	Anorthosite	ca. 1300 Ma	56° 29' 44" N	61° 36' 50" W	Nain plutonic suite	From local quarry; Not dated directly; has iridescent labradorite crystals
17CXA-D015	Monzogranite	ca. 1350 Ma	55° 28' 37" N	61° 28' 44" W	Nain plutonic suite	Part of the Mesoproterozoic AMCG-type intrusions in Labrador
17CXA-D017	Tonalite/granodiorite	(U-Pb dating in progress)	55° 48' 13" N	60° 29' 11" W		Crustal melt
17CXA-D018A1	Tonalitic gneiss	Likely ca. 2.8 Ga (U-Pb in progress)	55° 27' 40" N	60° 13' 28" W		Maggo gneiss
17CXA-D119	Pillow basalt	~ 1.88 Ga	55° 03' 00" N	66° 06' 40" W	New Quebec Orogen; Doublet Terrane	Tholeiitic volcanic rock; possible continental back-arc basin
18CXA-D041	Migmatitic orthogneiss, tonalitic	ca. 3258 Ma	55° 35' 11" N	60° 23' 42" W	North Atlantic Craton	Hopedale Block; Maggo Gneiss

5. Methodology

5.1. Sample preparation

Bedrock samples were cut into one section for bulk isotopic abundance analysis and major and trace element testing and another for thin section analysis. Bulk Re-Os sections were cut to include multiple characteristic features in order to be representative of overall rock composition. Thin section samples were cut to fit a 27 x 46 mm glass slide. Samples were polished to remove any saw marks and allowed to dry for at least 3 days. Bulk Re-Os sections were broken into smaller pieces using a hammer and powdered in a Zirconia ceramic grinding container using a shatterbox to a fine (~30 d) powder. Approximately 40 g of powder were collected for each rock sample.

5.2. Bulk rock Re-Os concentration and isotopic composition analysis

5.2.1. Rhenium isotopic abundances

Re isotopic concentrations were first measured on an iCAP Quad inductively coupled plasma mass spectrometer (ICP-MS). An inverse aqua regia digest was used to dissolve the Re in each sample. Briefly, ~0.1 g of powder from each sample was weighed out into a 22 mL glass vial. Samples were spiked with 10 µL of a mixed ^{185}Re-^{190}Os tracer solution to calibrate the sample's unknown abundance against a quantity of know Re and Os isotopic abundances. 6 mL of ~16 HNO_3 and 3 mL of ~12N HCl were added to each vial. After reacting without lids for 10 minutes, vials were capped and inverted to mix. Samples were placed on a hot plate at 120˚C overnight. The next morning, samples were removed from the hotplate and allowed to cool for 30 minutes. Solutions were then transferred to 15 mL centrifuge tubes and centrifuged for 3 minutes. After cleaning the vials, aqua regia was pipetted back into its corresponding vial and left on the hot plate to dry down overnight at 120˚C.

Re was isolated from inverse aqua-regia digested samples using solvent extraction. Samples were removed from the hot plate and allowed to cool. 5 mL of 5N NaOH were added to dried samples and left to react for 30 minutes. The sodium hydroxide and aqua regia solid were transferred to 15 mL centrifuge tubes and 5 mL of acetone were added. Solutions were agitated for a few minutes to ensure complete mixing. Samples were centrifuged for 3 minutes and the Re-bearing acetone was pipetted off the top into small PMP beakers. Acetone was evaporated on a hot plate at 60˚C overnight. The following day, dried samples were brought up in 4 mL of 0.8N

HNO_3, allowed to sit for 30 minutes, and transferred to 15 mL centrifuge tubes. Samples were run through iCAP ICP-MS and Re abundances were measured.

5.2.2. Rhenium and osmium isotopic abundances and compositions

Re and Os isotopic abundances and compositions were measured using negative thermal ionization mass spectrometry (N-TIMS). Approximately 0.1 g of each powdered sample was loaded into labelled Carius tubes with exact weights recorded. About 0.015 g of Spike #5 was added to each sample. A blank was created by adding ~0.020 g of Spike #2 to a Carius tube without powder. The Carius tubes were placed in a slurry of dry ice and ethanol. Inverse aqua regia, containing 6 mL of 15N NO_2 and 3 mL of 12N HCl, was added to each tube to aggressively break down silicate minerals and access the Os. Samples were left to freeze in the ice slurry.

Once frozen, the Carius tubes containing the samples were sealed. Using a gas and oxygen torch, the neck of each Carius tube was heated for about 10 seconds to remove moisture. The end of a glass sealing rod was heated until a melted blob formed. This blob was then pressed firmly onto the top of the Carius tube to seal it. A spot ~2 cm below the rim of the tube was heated. A pop indicated a good seal. The middle of the neck of the tube was then heated, allowed to collapse on itself and seal, and the sealing rod and top of the tube were pulled. Once sealed, the tubes were allowed to return to room temperature. Tubes were placed in the oven and the temperature was raised to 200˚C over the course of 2 hours. Samples were left in the oven for 48 hours.

After removing them from the oven, Carius tubes were etched around the body of the tube and placed in a slurry of dry ice and ethanol. Once frozen, the neck of the tube was heated with a torch to create a small hole. The end of the glass rod was heated and placed against the etched area to cleanly crack the tube along the etching. Tubes were transferred to the clean lab and 3.5 mL of $CHCl_3$ from 15 mL centrifuge tubes were transferred to the sample tubes. Once thawed, samples were transferred to corresponding 50 mL centrifuge tubes and agitated on the vortex. Samples were then transferred to a room temperature water bath for ~15 minutes. The chloroform containing the Os settled at the bottom of each tube and was transferred to 22 mL glass vials containing 3 mL of 9N HBr. Os extraction was repeated for each sample twice more. Once complete, vials were sealed and placed on the rocker overnight.

The next morning, vials were removed from the rocker. For each sample, the concave side of a watch glass was covered in Teflon tape. Enough 6N HCl was put on each watch glass to cover the tape, and watch glasses were placed on the hot plate at 40% for 1-2 hours. After cooled again, HCl was disposed of and the Os-bearing HBr was pipetted from each glass vial onto the corresponding watch glass. Os-bearing HBr was evaporated on the hot plate at 80˚C until ~20 µL were left. The 20 µL drop was transferred to the cap of the corresponding 22 mL glass vial. The caps were placed back on the hot plate and the samples were dried down over 30-60 minutes. After cooling for ~5 minutes, the caps were covered in parafilm and stored until run through the mass spectrometer.

On the day the N-TIMS was loaded, Os-micro distillation was performed on the samples. Two pieces of parafilm were cut. For each sample, 30 µL of CrO_3-H_2SO_4 and 20 µL 9N HBr were placed on the corresponding parafilm piece. Tristar vials were labelled, and 20 µL of 9N HBr was placed directly in the bottom of each. Vials were inverted. Parafilm was removed from the white caps and 50 µL of CrO_3-H_2SO_4 were added. Tristar vials were carefully sealed onto the white lids and placed on the hot plate at setting "M" (80˚C). The hotplate was covered with a Tupperware and left for 3-4 hours. Samples were removed and allowed to cool for 5-10 minutes. The Tristar vial was unscrewed from the white cap and inverted over a 10 cm strip of parafilm. Vials were placed back on the hot plate and allowed to dry down until ~1 µL of the HBr solution remained. Samples were then covered and taken to the TIMS lab for loading onto the Pt filaments.

5.3. Thin sections

Thin section samples were labelled, bagged, and mailed to Spectrum Petrographics in Vancouver, WA. There, samples were mounted on slides, ground down to a thinness to enable the transmission of optical light, and polished. The thin sections were mailed back to the lab. The intention was to analyze them under a microscope to better determine the rock type and mineral composition, but this analysis was never completed due to the COVID-19 outbreak and subsequent lab closure. The thin sections will be analyzed in the lab at a later time.

5.4. Major, minor, and trace element analysis

Samples were sent to Actlabs for major and trace element analysis. ~10 g of powder for each sample were placed in 15 mL centrifuge tubes and labelled. Samples were then shipped to Actlabs where they were analyzed for major and minor oxides and certain trace elements using lithium metaborate-tetraborate robotic fusion and inductively coupled plasma emission spectroscopy (ICP-FUS) and additional trace elements using inductively couple plasma mass spectrometry (ICP-MS). In the selected package, the major and minor elements tested for included SiO_2, Al_2O_3, Fe_2O_3, MnO, MgO, CaO, Na_2O, K_2O, TiO_2, and P_2O_5. Trace element analysis included Sc, Be, V, Ba, Sr, Y, Zr, Cr, Co, Ni, Cu, Zn, Ga, Ge, As, Rb, Nb, Mo, Ag, In, Sn, Sb, Cs, La, Ce, Pr, Nd, Sm, Eu, Gd, Tb, Dy, Ho, Er, Tm, Yb, Lu, Hf, Ta, W, Tl, Pb, Bi, Th, and U. Major and minor elements were reported using mass fraction in wt% and trace elements had units of ppm.

6. Results

6.1. Bulk osmium concentrations

Bulk Os concentrations ranged from 0.98 to 79.90 ppt. Concentrations tended to vary according to rock type. Mafic rocks, iron and magnesium rich rocks with SiO_2 < 65 wt%, generally had higher concentrations of Os and accompanying elements than felsic rocks with Si > 65 wt%. Igneous rocks had [Os] from 1.20 to 79.90 ppt. The mafic (basic) igneous rocks (pillow basalt and gabbro) had the highest values of 79.90 ppt and 56.90 ppt respectively. Felsic (acidic) igneous rocks (megacrystic granite, monzogranite, and anorthosite) contained less Os, from 1.20 to 13.50 ppt. Metasedimentary rocks (psammo-pelite, meta-siltstone, and grey quartzite) contained between 1.29 and 41.9 ppt of Os. Metaigneous rock samples (tonalitic orthogneiss) had [Os] of 0.98 ppt and 3.41 ppt. Bulk Re concentrations were low (0 – 0.1 ppb) for all samples.

Table 2: Bulk Os rock compositions. Data for 14 values was obtained before lab closure due to COVID-19. Missing are 14CXA-D30c, 17CXA-D119, and 18CXA-D041. Samples in gray italics were excluded from further analysis as outliers because $^{187}Os/^{188}Os$ uncertainties were high (> 0.1) or bulk Os concentrations were low (< 1 ppt).

Sample Name	Rock Type	Re (ppb)	±	Os (ppt)	±	192 Os (ppt)	±	$^{187}Os/^{188}Os$	±	Os at 20 kyr
14CXA-D072	Megacrystic granite	0.1	0.0	13.50	0.20	4.20	0.10	2.679	0.062	2.68
14CXA-D076	*Megacrystic granite*	*0.1*	*0.0*	*1.20*	*0.10*	*0.40*	*0.10*	*1.227*	*0.245*	*1.23*
14CXA-D097	*Tonalitic orthogneiss*	*0.1*	*0.0*	*4.40*	*0.20*	*0.60*	*0.10*	*15.455*	*2.099*	*15.45*
14CXA-D99	Gabbro	0.1	0.0	56.90	0.20	22.80	0.10	0.338	0.003	0.34
14CXA-D102	Meta-siltstone	0.1	0.0	41.90	0.20	17.20	0.10	0.193	0.002	0.19
15CXA-D002	Pillow basalt	0.1	0.0	79.90	0.50	24.40	0.10	2.829	0.020	2.83
15CXA-D005	Psammo-pelite	0.1	0.0	16.00	0.20	5.20	0.10	2.146	0.037	2.15
16CXA-D051	Psammo-pelite	0.0	0.0	15.58	0.11	6.18	0.09	0.442	0.008	0.44
16CXA-D065	Migmatitic orthogneiss, tonalitic	0.0	0.0	3.41	0.10	1.25	0.08	1.058	0.071	1.06
16CXA-D067	Grey quartzite	0.0	0.0	1.29	0.09	0.51	0.08	0.392	0.076	0.39
17CXA-D001	*Anorthosite*	*0.0*	*0.0*	*2.47*	*0.13*	*0.57*	*0.08*	*6.311*	*0.948*	*6.31*
17CXA-D015	*Monzogranite*	*0.0*	*0.0*	*1.41*	*0.09*	*0.49*	*0.08*	*1.664*	*0.284*	*1.66*
17CXA-D017	*Tonalite/granodiorite*	*0.0*	*0.0*	*5.12*	*0.29*	*0.40*	*0.08*	*32.878*	*6.692*	*32.88*
17CXA-D018A1	*Tonalitic gneiss*	*0.0*	*0.0*	*0.98*	*0.09*	*0.39*	*0.08*	*0.386*	*0.099*	*0.39*

6.2. Osmium isotopic compositions

Os isotopic compositions (IC) ranged widely from 0.193, below average continental crust compositions, to 32.878, well above crustal averages (Table 2). Samples with IC uncertainty values greater than ± 0.1 were excluded from further analysis. Another spike with different concentrations of Os will be used to retest these samples at a later date, allowing for better calibration of the Os naturally present in the sample. Sample 17CXA-D018A1 was also excluded from further analysis because its bulk Os concentration was less than 1 ppt. A rock with such a low Os concentration after digestion in a strong, acidic solution would be expected to contribute no Os under typical weathering conditions by weakly acidic rainwater and glacial meltwater. Samples with similarly low bulk Os concentrations (16CXA-D065 and 16CXA-D067) were included in analysis due to their low IC uncertainties but should be considered similarly small contributors to the marine Os reservoir. This left 8 samples (14CXA-D072, 14CXA-D99, 14CXA-D102, 15CXA-D002, 15CXA-D005, 16CXA-D051, 16CXA-D065, and 16CXA-D067) for consideration in this study, comprised of igneous, metaigneous, and metasedimentary rock types. Bulk Os concentrations of these 8 samples were from 1.29 to 79.90 ppt.

There was no correlation between Os IC and bulk Os concentration (Figure 7). Igneous, metaigneous, and metasedimentary rocks followed no distinct pattern. The pillow basalt (15CXA-D002) had both the highest bulk Os concentration (79.90 ppt) and the highest Os IC (2.829) of the samples considered here. However, although the gabbro sample (14CXA-D99) also had a high bulk Os content (56.90 ppt), it had a relatively low IC (0.338). Conversely, the megacrystic granite (14CXA-D072) had a lower bulk concentration (13.50 ppt) but a high radiogenic signature (2.679).

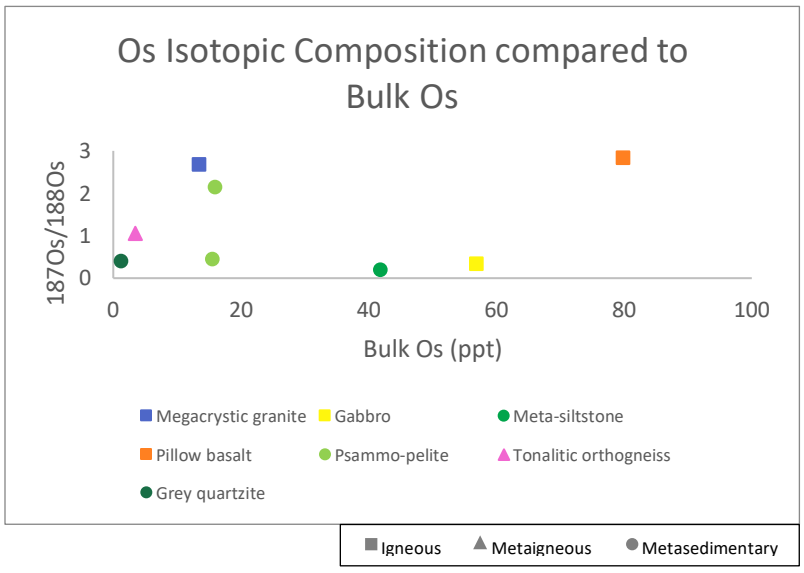

Figure 7: Os radiogenic isotopic composition compared to bulk Os concentration. The amount of Os in the sample does not appear to affect the $^{187}Os/^{188}Os$ values in a uniform way across samples. The igneous (square), metaigneous (triangle), and metasedimentary (circle) characterization of the sample also does not seem to have an effect.

There was no significant correlation between sample age and isotopic composition or bulk Os concentration (Figure 8). All samples were Archean or early Proterozoic in age and those analyzed were roughly estimated to be between 1.83 and 2.6 billion years old. Two of the youngest samples, the pillow basalt (1.88 Ga) and the psammo-pelite (1.83 Ga), had ICs on the higher end of the rocks samples (2.829 and 2.146 respectively). The megacrystic granite sample (2.3 Ga) also had a high IC value (2.679). Most of the metasedimentary samples had lower ICs (0.193 – 0.442) except for the psammo-pelite sample with a value of 2.146. Igneous rock types ranged in age (1.88 – 2.3 Ga) and IC (0.338 – 2.829). The metaigneous sample was the oldest (2.6 Ga) and had an IC of around 1.058.

Bulk Os concentrations overall also followed no discernable pattern with concern to sample age (Figure 8). Igneous rocks may have had increased [Os] for younger samples, but the limited number of data points makes it difficult to tell. Additionally, this trend may more significantly reflect individual rock compositions within the igneous subgroup because the pillow basalt and gabbro samples were the two igneous samples with the highest [Os]. Bulk Os in metasedimentary samples ranged from 1.29 to 41.9 ppt for meta-siltstone and grey quartzite samples (2.167 Ga) and from 15.58 to 16.00 ppt for psammo-pelite samples (1.83 Ga). The metaigneous tonalitic orthogneiss sample (2.6 Ga) had a low bulk Os concentration (3.41 ppt).

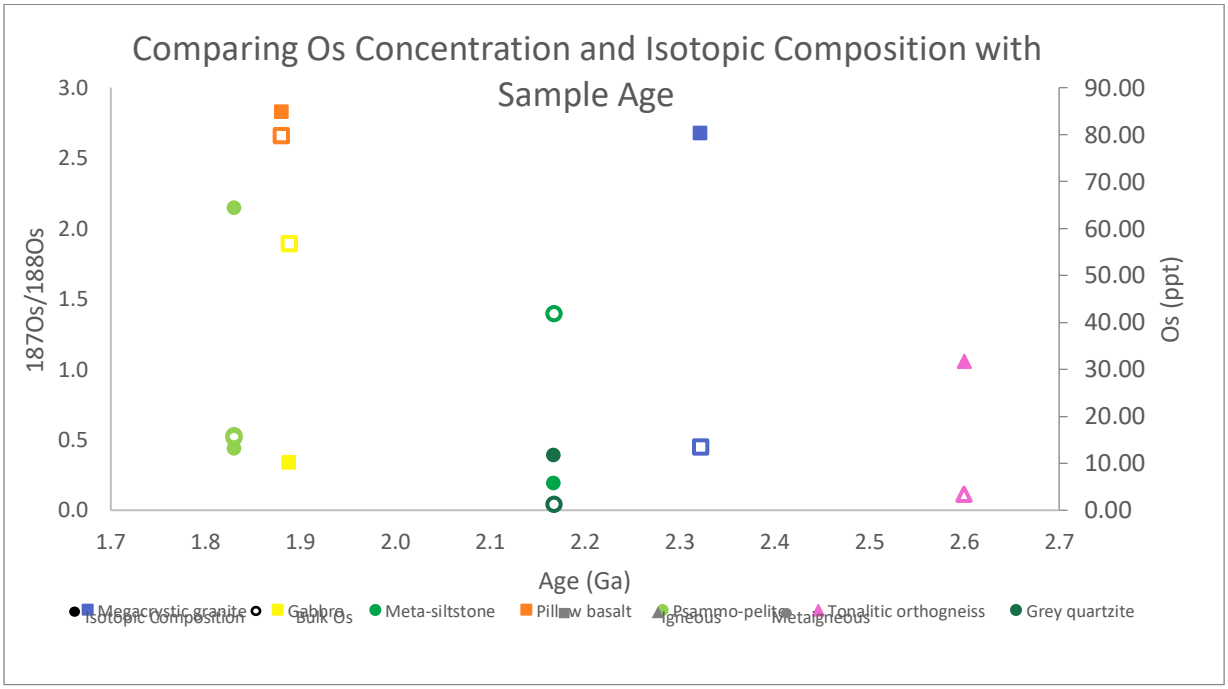

<u>Figure 8:</u> Os radiogenic isotopic composition and bulk Os concentration compared to sample age. Solid markers correspond to the $^{187}Os/^{188}Os$ primary vertical axis on the left, and empty markers refer to the [Os] (ppt) secondary vertical axis on the right. Square markers correspond to igneous rock types, triangles to metaigneous, and circles to metasedimentary. Neither isotopic composition nor concentration seem to be determined by sample age.

6.3. Major, minor, and trace elements

Major and minor elements varied across rock types (Table 3, Figure 9). Meta-siltstone, tonalite/granodiorite, grey quartzite, tonalitic orthogneiss, and megacrystic granite all had averaged SiO_2 mass fractions greater than 65% of the total rock, characterizing them as felsic. Psammo-pelite and monzogranite samples were intermediate, with silica averages between 55% and 65%. With silica averages between 45% and 55%, anorthosite, pillow-basalt, and gabbro samples were mafic. Rock types high in plagioclase feldspar (tonalitic orthogneiss, gabbro, pillow basalt, anorthosite, tonalite/grandiorite) had correspondingly elevated levels of CaO, Na_2O, and/or MgO. Rock types with a large ferromagnesian component (pillow basalt, gabbro, anorthosite, grey quartzite) had high concentrations of Fe_2O_3 and MgO.

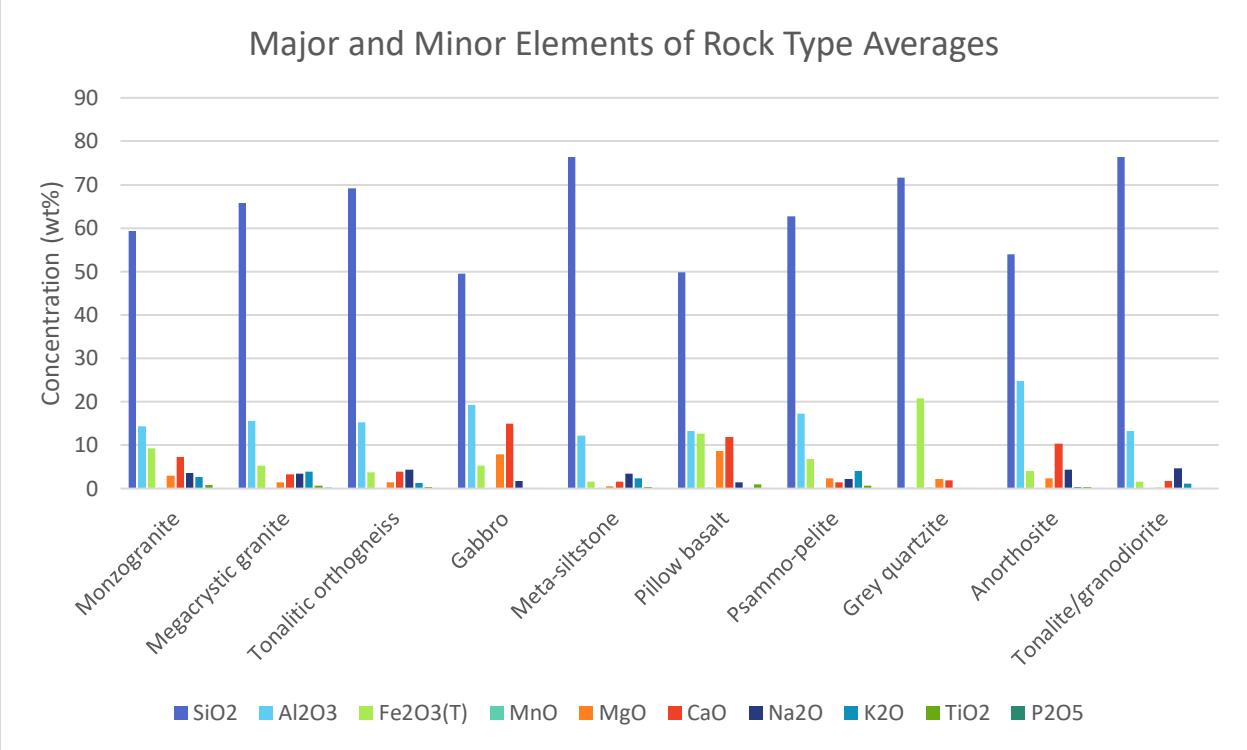

<u>Figure 9:</u> Major and minor element concentrations averaged across rocks of the same classification. MEs vary according to rock type.

Major and minor elements were also consistent across samples of the same rock type (Figure 10). For megacrystic granite, pillow basalt, and psammo-pelite, samples were with in 5 wt% of each other in SiO_2 concentration. The range was larger (within 20 wt%) for the monzogranite and tonalitic orthogneiss samples. All other major and minor elements for each rock type were within 5 wt% of each other, with the exception of one monzogranite sample (14CXA-D30c). This monzogranite sample had a lower silica concentration and higher levels of Fe_2O_3, MgO, and CaO.

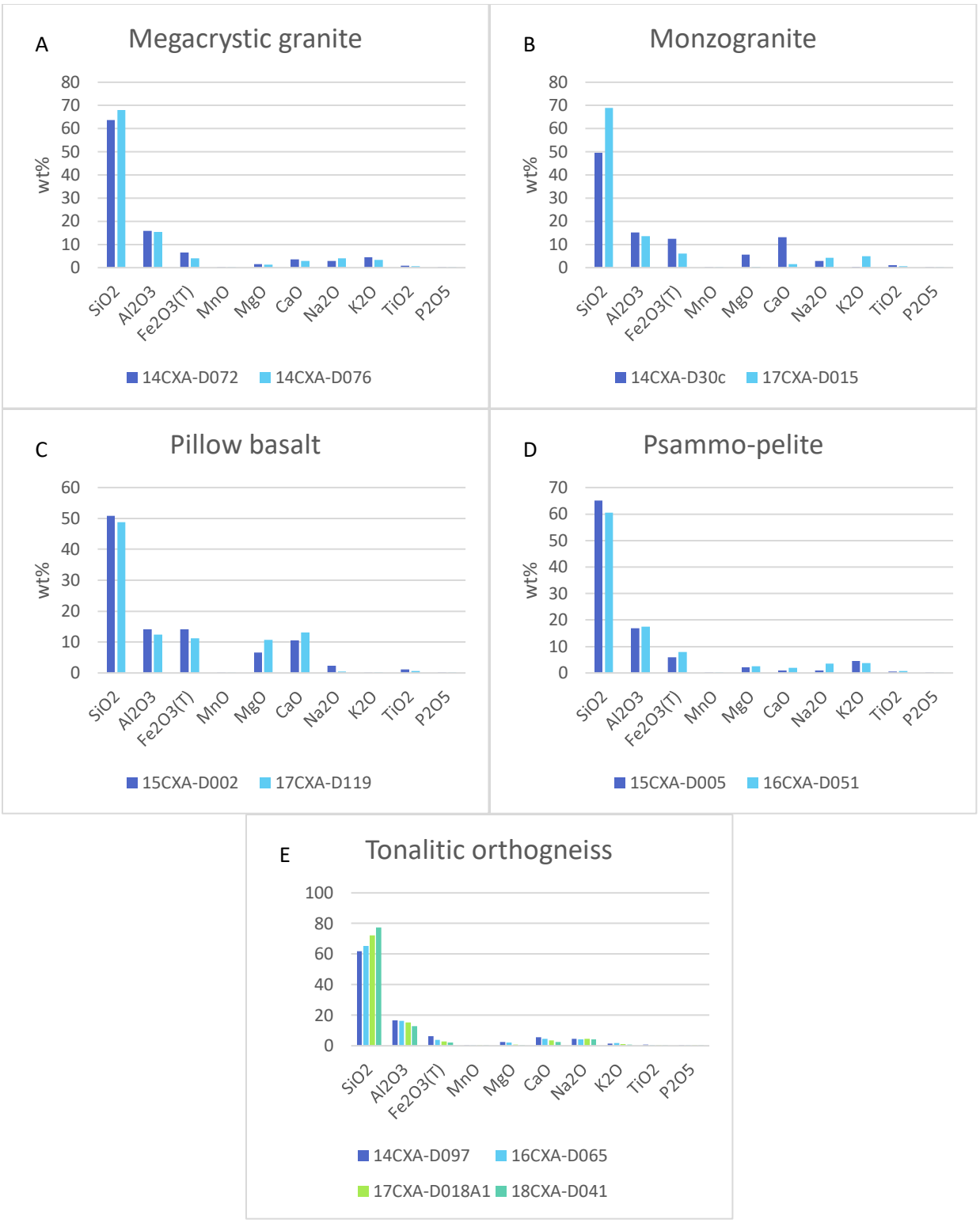

Figure 10: A comparison of samples of the same rock type for (A) megacrystic granite, (B) monzogranite, (C) pillow basalt, (D) psammo-pelite, and (E) tonalitic orthogneiss. All other rock types analyzed in this study only had one sample. MEs are fairly consistent between samples of the same rock type, with the exceptions of the monzogranites and the tonalitic orthogneisses.

Table 3: Major and minor elements. Samples were processed on 1/20/2020 by Actlabs using FUS-ICP. Values represent % by volume.

Analyte Symbol		SiO2	Al2O3	Fe2O3(T)	MnO	MgO	CaO	Na2O	K2O	TiO2	P2O5
Detection Limit		0.01	0.01	0.01	0.001	0.01	0.01	0.01	0.01	0.001	0.01
14CXA-D072	Megacrystic granite	49.67	15.22	12.46	0.191	5.72	13.03	2.95	0.39	1.116	0.09
14CXA-D076	Megacrystic granite	63.66	15.79	6.52	0.096	1.52	3.63	2.79	4.51	0.795	0.2
14CXA-D097	Tonalitic orthogneiss	68.02	15.33	3.99	0.065	1.3	2.81	4.02	3.42	0.653	0.17
14CXA-D99	Gabbro	61.91	16.61	6.16	0.1	2.42	5.52	4.39	1.38	0.669	0.17
14CXA-D102	Meta-siltstone	49.44	19.25	5.3	0.108	7.92	15.01	1.75	0.03	0.152	< 0.01
15CXA-D002	Pillow basalt	76.32	12.18	1.61	0.091	0.5	1.63	3.4	2.41	0.4	0.05
15CXA-D005	Psammo-pelite	50.9	14.19	14.07	0.204	6.59	10.57	2.34	0.2	1.22	0.09
16CXA-D051	Psammo-pelite	65.09	16.97	5.83	0.035	2.11	0.91	0.96	4.49	0.528	0.06
16CXA-D065	Migmatitic orthogneiss, tonalitic	60.43	17.45	7.95	0.117	2.5	2.03	3.5	3.63	0.813	0.2
16CXA-D067	Grey quartzite	65.2	16.33	3.97	0.075	2.27	4.53	4.31	1.66	0.466	0.12
17CXA-D001	Anorthosite	71.56	0.21	20.85	0.179	2.26	1.87	0.07	0.06	0.002	< 0.01
17CXA-D015	Monzogranite	53.91	24.84	4.07	0.056	2.3	10.33	4.43	0.38	0.297	0.02
17CXA-D017	Tonalite/granodiorite	68.86	13.59	5.99	0.098	0.31	1.5	4.36	5.02	0.558	0.1
17CXA-D018A1	Tonalitic gneiss	76.31	13.25	1.54	0.022	0.21	1.77	4.64	1.07	0.089	0.02

Table 4: Trace elements. 18 of the 45 elements test for are listed here. Samples were processed on 1/20/2020 by Actlabs. Values represent measured in ppm. Samples were analyzed using either FUS-ICP or FUS-MS. Blue corresponds to siderophilic elements, red to chalcophilic, and gray to lithophilic.

Analyte Symbol	Sc	Ba	Zr	Cr	Co	Ni	Cu	Zn	Ga	Ge	Ag	Sn	Nd	Sm	Tl	Pb	Th	U
Detection Limit	1	2	2	20	1	20	10	30	1	1	0.5	1	0.1	0.1	0.1	5	0.1	0.1
Analysis Method	ICP	ICP	ICP	MS	MS	MS	MS	MS	MS	MS	MS	MS	MS	MS	MS	MS	MS	MS
14CXA-D072	14	2085	373	30	13	< 20	20	80	19	1	1	1	37.1	6.3	0.6	15	6.7	0.6
14CXA-D076	10	1304	311	20	6	< 20	< 10	70	21	1	0.8	1	46.6	8.1	0.7	21	6.4	0.6
14CXA-D097	13	153	170	40	17	40	< 10	100	21	1	< 0.5	2	14.1	3.2	0.5	9	1.8	1
14CXA-D99	33	12	99	350	26	100	20	< 30	12	2	< 0.5	< 1	0.8	0.3	< 0.1	< 5	< 0.1	< 0.1
14CXA-D102	5	448	494	30	3	< 20	170	< 30	12	2	1.4	1	24.6	3.9	0.3	16	9	1.6
15CXA-D002	49	48	114	180	50	110	60	110	15	2	< 0.5	1	7.6	2.6	< 0.1	< 5	0.2	0.1
15CXA-D005	12	871	211	90	12	30	30	70	22	2	0.6	1	31.1	5.1	0.7	12	11.7	1.7
16CXA-D051	18	606	231	100	17	60	< 10	120	19	2	0.6	2	2.5	0.8	0.7	23	7.9	2.4
16CXA-D065	9	777	203	50	13	50	20	80	17	< 1	0.7	1	13	2.6	0.3	24	2.3	1
16CXA-D067	< 1	17	90	< 20	1	< 20	< 10	< 30	< 1	5	< 0.5	< 1	0.3	< 0.1	< 0.1	< 5	< 0.1	< 0.1
17CXA-D001	8	285	168	60	13	20	< 10	30	20	< 1	0.5	< 1	2.5	0.5	< 0.1	< 5	< 0.1	< 0.1
17CXA-D015	7	979	1072	< 20	2	< 20	< 10	160	26	2	3	6	105	18.2	0.6	30	13.3	1.5
17CXA-D017	< 1	214	298	< 20	1	< 20	< 10	30	15	< 1	0.8	1	16.3	2	0.2	9	5.7	0.4
17CXA-D018A1	3	176	379	< 20	5	< 20	< 10	60	16	< 1	1	1	11.4	1.8	0.2	6	2.8	0.3

There were clear differences in the concentration of key trace and minor elements in mafic rocks as compared to felsic rocks (Table 4). All siderophilic and chalcophilic elements as well as an assortment of lithophilic elements were examined. Figures 11 and 12 illustrate the examples with the most visible trends. Nd, Sm, Th, and U were more concentrated in rocks of felsic composition (Figure 11). Cr, Ni, TiO_2, Sc, Co, and Os were more concentrated in mafic rocks with lower silica concentrations (Figure 12).

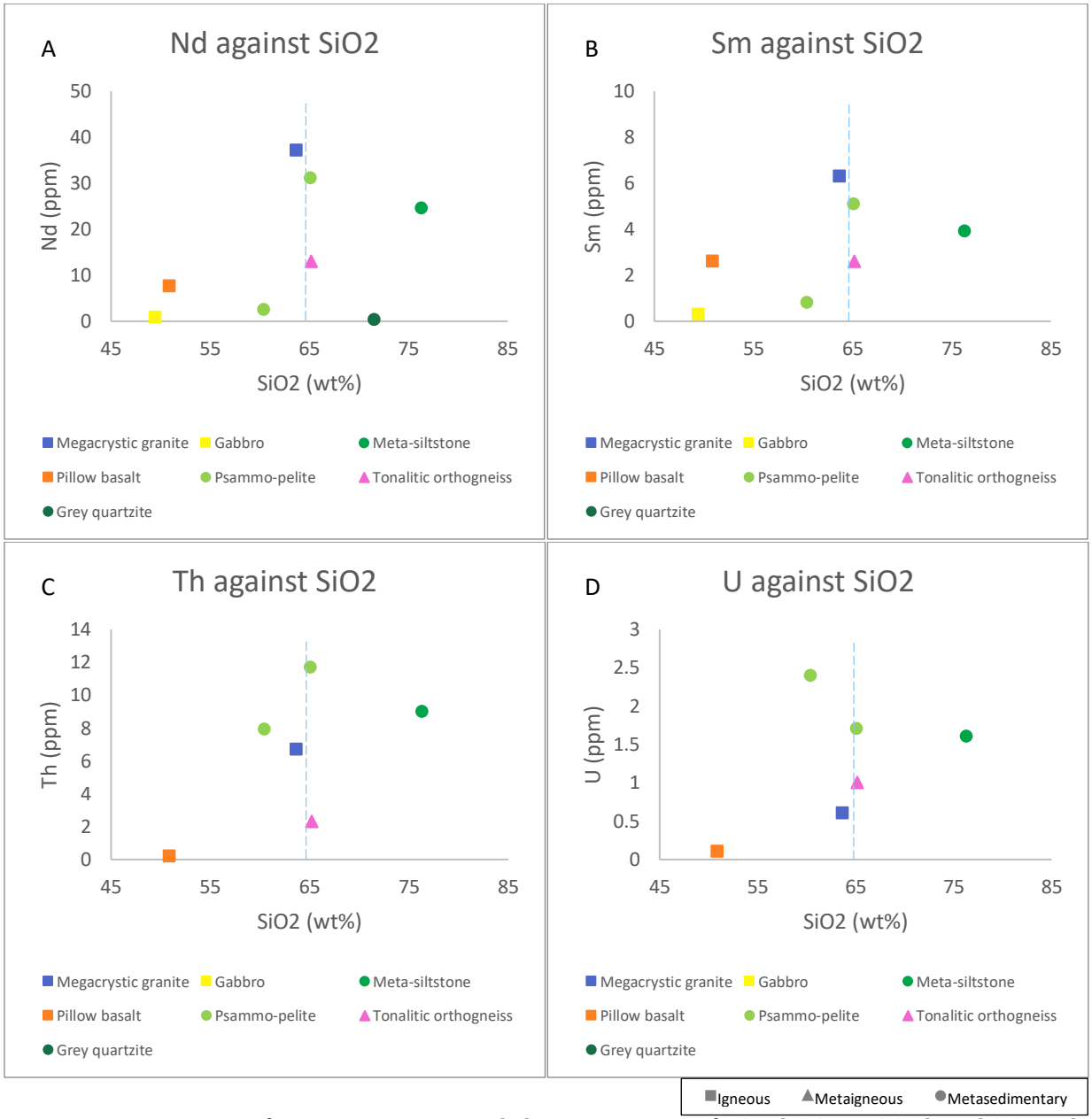

Figure 11: A comparison of SiO_2 concentrations with the concentrations of (A) Nd, (B) Sm, (C) Th, and (D) U. The blue dotted line at 65 wt% silica represents the cutoff between mafic and felsic rock types. These four trace elements showed an increase in concentration for more felsic samples.

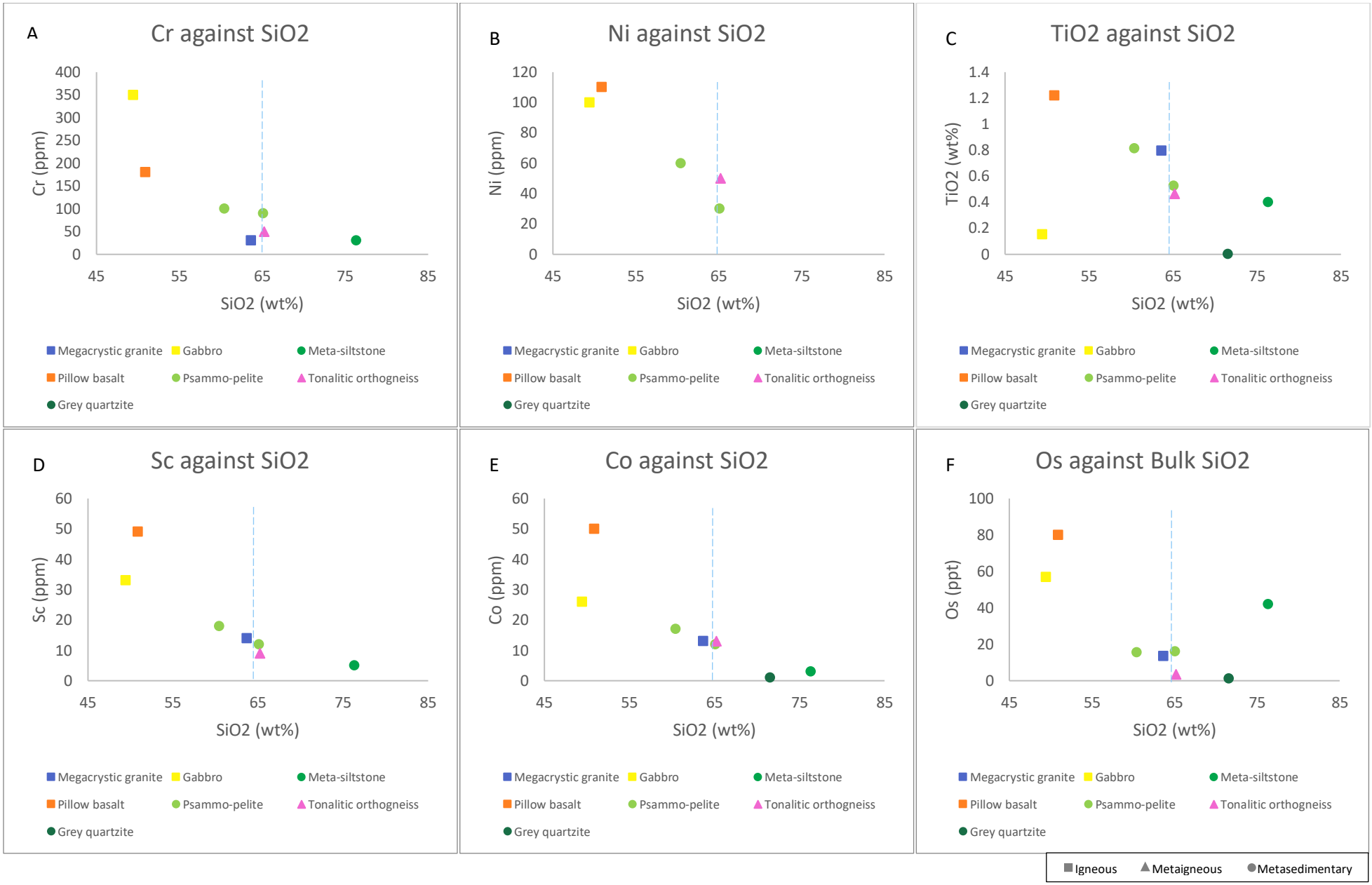

Figure 12: A comparison of SiO_2 concentrations with the concentrations of (A) Cr, (B) Ni, (C) TiO_2, (D) Sc, (E) Cp, and (F) Os. The blue dotted line at 65 wt% silica represents the cutoff between mafic and felsic rock types. These six trace elements showed an increase in concentration for more mafic samples.

6.4. Elemental abundances compared to bulk osmium concentrations

Certain elements appear to be more strongly associated with Os in the bedrock samples than do others. Of the major elements analyzed, SiO_2 revealed a weak trend when compared with bulk Os content (Figure 13). As discussed previously, felsic rocks with a high silica mass fraction tended to have lower bulk Os concentrations, while mafic rocks with silica mass fractions below 65 wt%, primarily the pillow basalt and gabbro rock types, had high [Os]. There did not appear to be a correlation between [Os] and [Fe_2O_3]. Although the pillow basalt had high concentrations of both elements, iron concentrations for the other rock types were variable and followed no clear trend. MnO and TiO_2, minor elements making up less than about 1 wt% of the rock, both showed slight positive correlations with [Os].

Weakly siderophilic trace elements measured included Co and Ni. These elements were positively correlated with bulk Os (Figure 14). Higher [Os] corresponded to higher concentrations in both of these elements. This was more pronounced when comparing [Os] with [Co]. The trend is still visible for nickel, but because [Ni] was below the detection limit for some of the samples with lower [Os], there are fewer data points.

Chalcophilic trace elements – including Cu, Zn, Ga, Ge, Ag, Sn, Tl, and Pb – showed no relationship to bulk Os concentration. For many of these elements, certain samples were below the detection limits, and available data was disparate.

Of the lithophilic trace elements studied, Sc and Cr both correlated positively with bulk Os concentration (Figure 15). Nd, Sm, Th, and U – all elements belonging to other commonly used radiogenic isotope systems – correlated negatively with bulk Os, tending to decrease in concentration as [Os] increased.

There was no relationship observed between Os isotopic composition and the concentrations of the siderophilic, chalcophilic, or lithophilic elements mentioned above. The radiogenic Os did not correspond to higher concentrations in the elements that were found to associate more readily with higher concentrations in bulk Os.

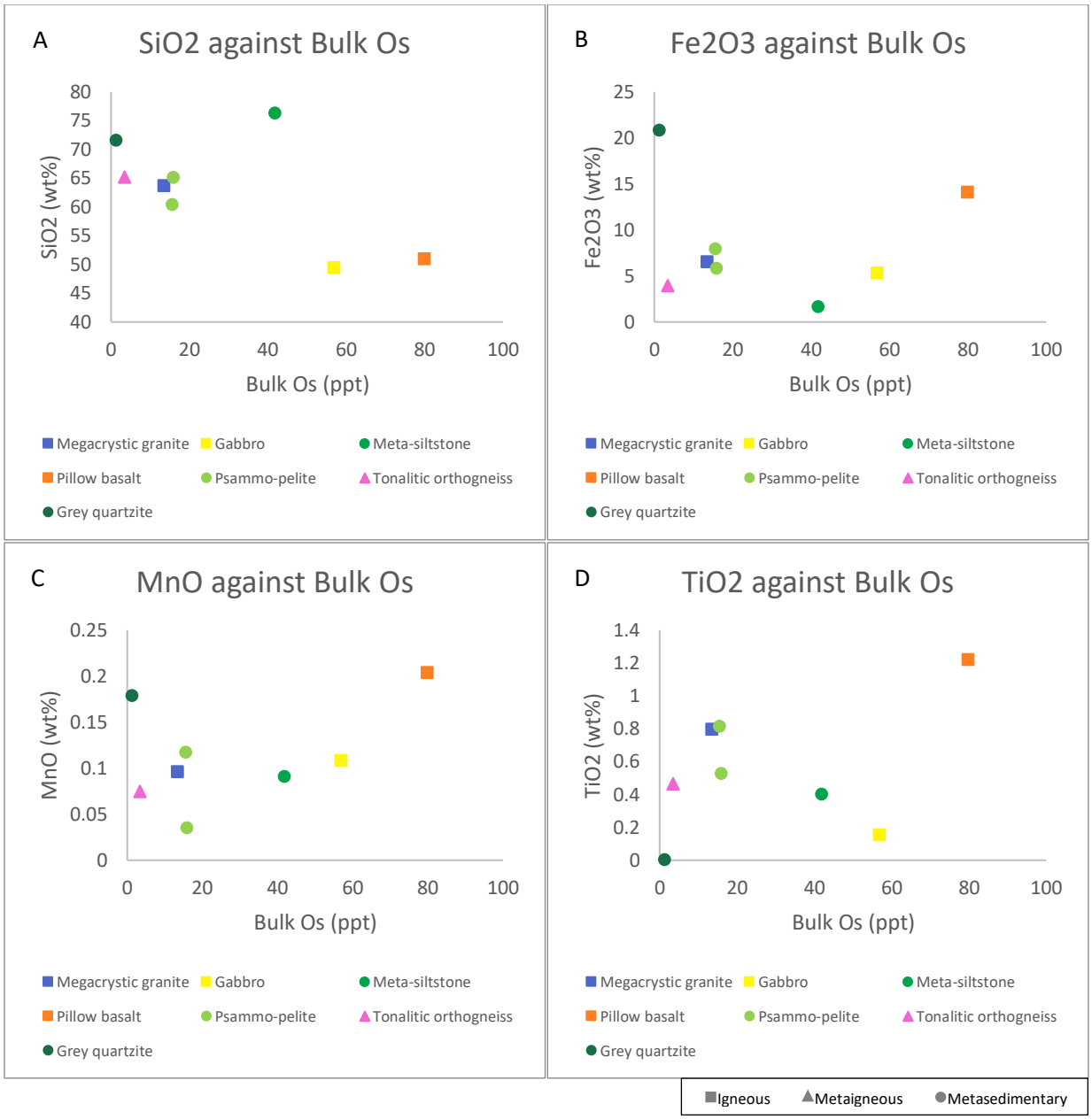

Figure 13: Major and minor elements (A) SiO_2, (B) Fe_2O_3, (C) MnO, and (D) TiO_2 compared to bulk Os concentrations. (A) [SiO_2] was weakly negatively correlated with increased [Os], and (C) [MnO] and (D) [TiO_2] both showed weak positive correlations with [Os].

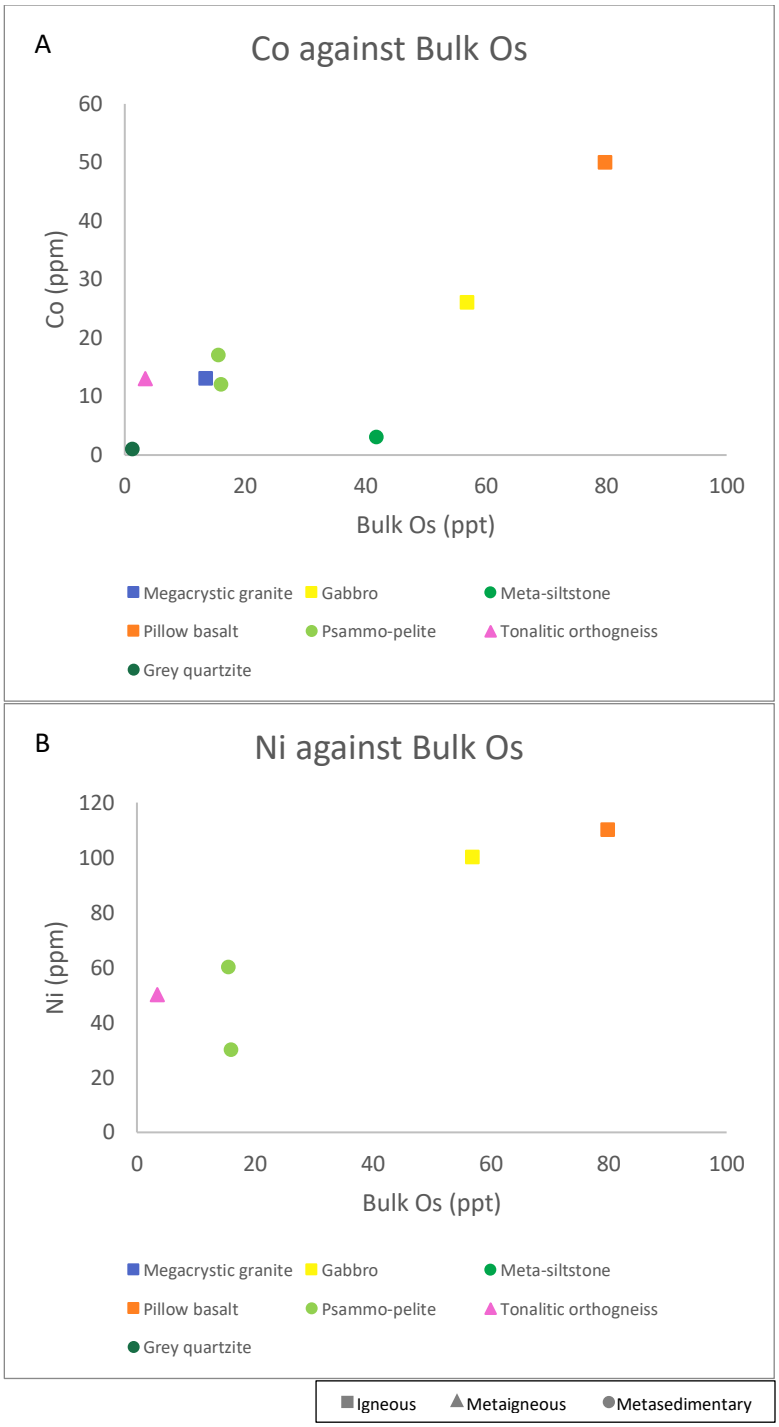

<u>Figure 14:</u> Siderophile trace elements (A) Co and (B) Ni compared to bulk Os concentrations. Both were positively correlated with increasing [Os].

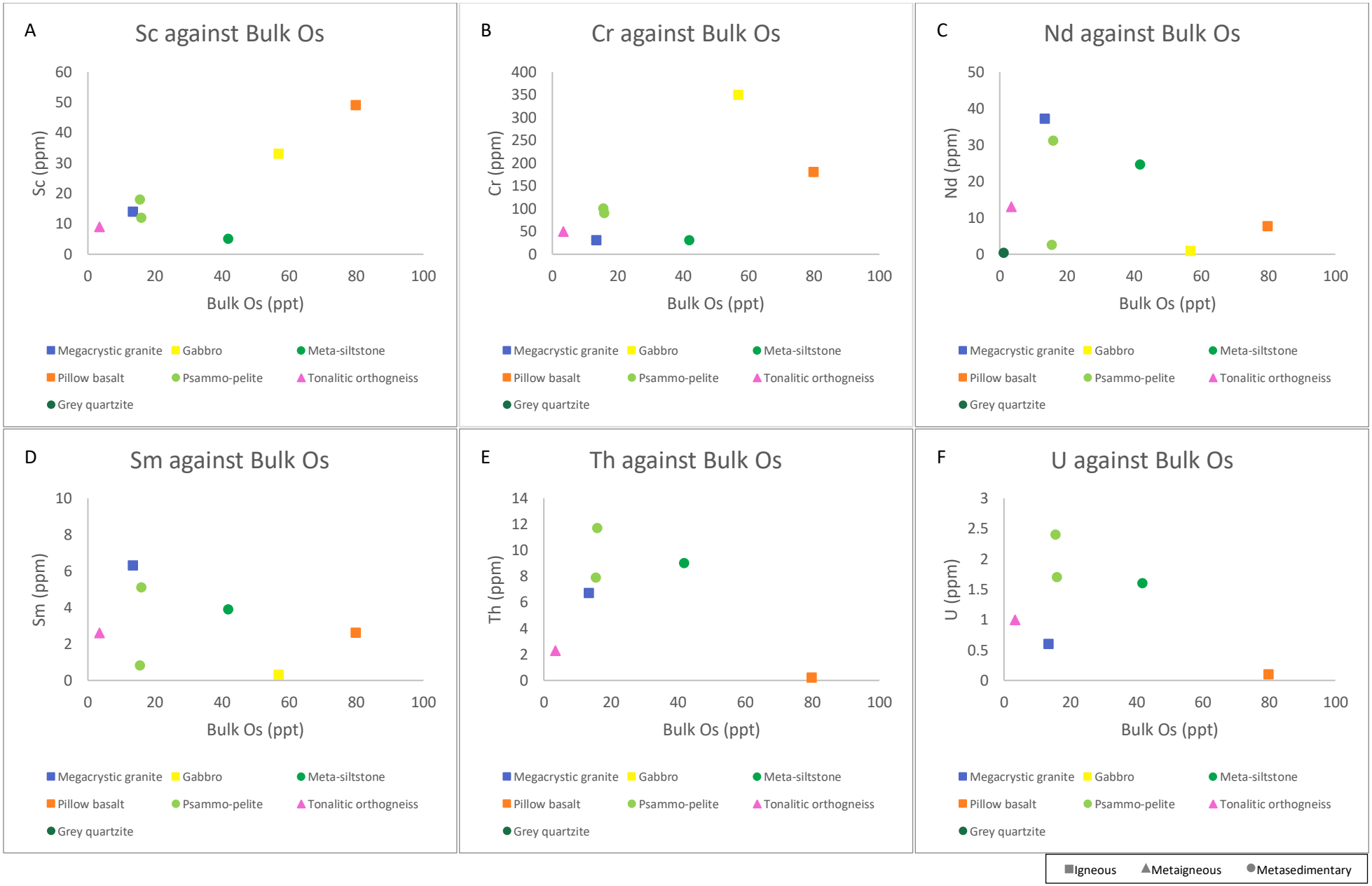

<u>Figure 15:</u> Lithophilic trace elements (A) Sc, (B) Cr, (C) Nd, (D) Sm, (E) Th, and (F) U compared to bulk Os concentrations. (A) [Sc] and (B) [Cr] were positively correlated with increased [Os]. (C) – (F), all elements belonging to other long-lived radiogenic isotope systems, showed slight negative correlations with increased [Os].

7. Discussion

7.1. Variations in osmium isotopic composition

The cratonic bedrock samples analyzed in this study had a wide assortment in Os isotopic compositions, from $^{187}Os/^{188}Os$ = 0.193 to 2.679. Samples with large values of $^{187}Os/^{188}Os$ are more radiogenic, as is expected of bedrock of this age. Typically, Re, compared to Os, is preferentially partitioned into crustal melt, resulting in higher concentrations of radiogenic Os than stable Os in rocks of Archean and early Proterozoic age like those studied here (Shirey and Walker, 1998). With values over 1, these samples contained more radiogenic ^{187}Os than stable ^{188}Os. Taken together with the low concentration of Re, it is clear that ^{187}Re that was initially incorporated into the rock at the time of formation has decayed into ^{187}Os.

Samples on the lower end of this range with values less than 1 are relatively unradiogenic. They contain less ^{187}Os than stable ^{188}Os. Given that four samples had $^{187}Os/^{188}Os < 1$, it is possible that other factors, such as conditions or mechanisms at the time of formation, may have resulted in more stable Os incorporated into these rocks at the time of melt, giving rise to a radiogenic signal of lesser magnitude today.

The Os ICs vary significantly from typical continental crust values of ~1.4. Weathering of these rocks by the Laurentide Ice Sheet and their incorporation into marine environments through ice rafted debris or glacial meltwater would release Os with radiogenic signatures distinct from typical riverine inputs (Peucker-Ehrenbrink and Ravizza, 2012). This would be expected to upset steady-state marine conditions. Such a change would be reflected in marine sediment cores in the North Atlantic Ocean.

Quantifying the variability of Os ICs in bedrocks from this area is an important step in characterizing transition periods of the LIS. Changes in weathering flux into the ocean would be reflecting in marine sediment cores at corresponding intervals. Such data could help us estimate rates of deglaciation at the end of glacial periods throughout the Pleistocene and at the end of the Last Glacial Maximum. Furthermore, the ICs of continental bedrock underlying the LIS may enable the confirmation of the regolith hypothesis. If the MPT occurred as a result of the LIS eroding a soft, regolith substrate to expose hard, crystalline bedrock like that studied here, as Clark and Pollard (1998) hypothesized, the North Atlantic sediment cores should reflect a shift from Os isotopic compositions of around 1.4 to the range in $^{187}Os/^{188}Os$ values observed in this

study. Analysis of marine sediment cores from the North Atlantic containing Os from IRD and organic matter has the potential to confirm this hypothesis.

7.2. Osmium isotopic compositions and sample age

Interestingly, although the radiogenic signal of a rock is expected to correlate with its age of formation, the samples studied here do not follow that trend. Typically, older samples have higher Os isotopic compositions because more ^{187}Re has decayed into ^{187}Os (Stein and Hannah, 2014). Because all of the rocks analyzed here are more than 1.83 billion years old, $^{187}Os/^{188}Os$ values would be expected to be high, greater than typical continental values of 1.4. This is not the case for all of the samples; several are an order of magnitude smaller. It is possible that mineralogy impacted the amount of Re initially incorporated into these samples at the time of formation, reducing the importance of age in determining the radiogenic IC of these samples.

However, because there was no general relationship observed between Os IC and elemental concentrations, it doesn't seem like rock type has a singular or easily characterized impact on the radiogenic signal of the samples tested. Igneous, metaigneous, and metasedimentary rock types all demonstrated a range in Os IC independent of sample age. This hints at the complexity underlying Re and Os incorporation into igneous rocks at the time of formation. The behavior of Re and Os during these processes is still poorly understood, leading to large uncertainties in ascertaining "normal" Re and Os abundances in mantle melts and typical Re and Os compatibility to modal mineralogy (Shirey and Walker, 1998). Re mantle hosts and variable behavior during melting, a growing field of study, are particularly important to further characterize for applications of the Re-Os system (Shirey and Walker, 1998). A better understanding of these processes might shed light on the variability in ICs of the samples in this study. In addition, the retesting of the samples with large uncertainties using different spikes and the analysis of additional samples may help shed light on the cause of this anomaly.

7.3. Re-Os application in mafic rock types

Os and other elements such as Co, Ni, TiO_2, Cr, and Sc were more concentrated in mafic rocks with silica concentrations < 65 wt%. Co, Ni, and Os, like other platinum group elements, are all siderophiles (Day et al., 2016). They partition preferentially into mafic rocks because of their higher iron and magnesium concentrations. TiO_2, Cr, and Sc behave similarly. This suggests that

Os can reliably be expected to have higher concentrations in rocks with lower silica contents and higher Co, Ni, TiO_2, Cr, and Sc concentrations. On the other hand, Nd, Sm, Th, and U were more concentrated in felsic rocks. Nd, Sm, Th, and U belong to other widely used long-lived radiogenic isotope systems, with applications in geochronology (Frank, 2002). However, due to their lower concentrations in mafic rocks, the application of these systems in these rock types can be limited. The Re-Os isotope system has the potential to work well as a proxy method particularly when dealing with mafic rocks like basalts and gabbros because of its siderophilic properties.

Further study of Re and Os abundances in mafic rocks at the time of formation is necessary to typify the behavior of Os in rocks with varying modal mineralogies. This is beyond the scope of this project, but our data does emphasize the importance of this research for applications of the Re-Os system in mafic rocks that have traditionally been difficult to study using other radiogenic isotope systems.

7.4. Osmium and associated elements

Os is strongly associated with certain elements. These elements include the other siderophiles measured in this study, Co and Ni. The siderophilic properties of these three elements likely caused all three to partition preferentially into rocks rich in iron, such as the mafic rocks analyzed here. Certain lithophilic elements like Sc and Cr also accompanied raised bulk Os concentrations. Such an association may be due to the types of metals all three elements are associated with and the alloys Os and other platinum group elements typically form. Bulk Os concentration appears to have little to no correlation with other chalcophile elements, suggesting that its chalcophilic nature is less important in determining its bulk concentration than its siderophilic properties. It is negatively correlated with other lithophilic elements as would be expected given its aversion to silica-rich rocks.

Testing for more commonly found elements may be an effective way to predict which rocks will have higher Os concentrations. Samples could be sent out for ME and TE evaluation prior to Os analysis to limit the number of samples run through the more costly and time-consuming procedure. However, although the bulk Os concentrations appear to depend on rock type and correlate to elements with similar properties, radiogenic isotopic compositions do not follow this trend. While bulk rock elemental abundances of more common elements may be a

useful predictor for bulk Os concentrations, they appear unhelpful in estimating the Os isotopic composition.

8. Conclusions and Future Work

Climate simulations require paleoclimate proxy data with large spatial and temporal distributions to inform how they model ice sheet dynamics and predict future sea level rise. The Re-Os isotope system is a promising geochemical proxy because it is able to indicate continental weathering sources and is applicable to rock types in which other radiogenic isotope systems are limited. The cratonic bedrock samples examined in this study have a wide range of radiogenic isotopic compositions and are expected to have upset steady-state marine isotopic conditions during the second half of the Pleistocene through glacial erosion and weathering by the Laurentide Ice Sheet. The mineralogy and elemental concentrations of these rocks highlight the significance of the siderophilic nature of Re and Os. Additionally, they emphasize the importance of the Re-Os system in applications for mafic rock types.

Further testing of the samples with low bulk Os concentrations and high isotopic composition uncertainties is necessary to determine the weathering contributions of these rocks. The survey undertaken in this study will support the work of doctoral student Erica Evans, a member of Dr. Alan Rooney's lab, in her study of the MPT and ice sheet dynamics during the Pleistocene. The cratonic bedrock isotopic signals will be compared to marine sediment cores from the North Atlantic to determine whether a shift from regolith to crystalline bedrock subglacial conditions occurred at the MPT.

9. Acknowledgements

I would like to thank Professor Alan Rooney for his guidance and support during this project and throughout the time I've worked in his lab. I am also grateful to Erica Evans, Lexie Millikin, and Sierra Anseeuw for their help in learning lab methods, executing the more technical parts of the procedures, and understanding some of the concepts underlying the methodology. I'd like to thank Professor Noah Planavsky for being a second reader and Professor Mary-Louise Timmermans for her encouragement and advice during her time as the Director of Undergraduate Studies of the Geology & Geophysics Department. This project was made

possible in part by the financial support provided by the Karen L. Von Damm ’77 Undergraduate Research Fellowships in Geology & Geophysics. I would also like to acknowledge the Juneau Icefield Research Program for inspiring my interest in cryosphere sciences and my research advisor, Dr. Brad Markle, for his enthusiasm during the program and his suggestions regarding background research for this project. Lastly, I would like to express my gratitude for my friends and family who supported me throughout this endeavor.

10. References

Andrews, J. T., & MacLean, B. (2003). Hudson Strait ice streams: A review of stratigraphy, chronology and links with North Atlantic Heinrich events. *Boreas*, *32*(1), 4–17. https://doi.org/10.1080/03009480310001010

Anorthosite. (2020). In *Wikipedia*. https://en.wikipedia.org/w/index.php?title=Anorthosite&oldid=950102281

Balco, G., & Rovey, C. W. (2010). Absolute chronology for major Pleistocene advances of the Laurentide Ice Sheet. *Geology*, *38*(9), 795–798. https://doi.org/10.1130/G30946.1

Bassis, J. N., Petersen, S. V., & Mac Cathles, L. (2017). Heinrich events triggered by ocean forcing and modulated by isostatic adjustment. *Nature*, *542*(7641), 332–334. https://doi.org/10.1038/nature21069

Canadian Shield | Definition, Location, Map, Landforms, & Facts | Britannica. (n.d.). Retrieved April 24, 2020, from https://www.britannica.com/place/Canadian-Shield

Chalk, T. B., Hain, M. P., Foster, G. L., Rohling, E. J., Sexton, P. F., Badger, M. P. S., Cherry, S. G., Hasenfratz, A. P., Haug, G. H., Jaccard, S. L., Martínez-García, A., Pälike, H., Pancost, R. D., & Wilson, P. A. (2017). Causes of ice age intensification across the Mid-Pleistocene Transition. *Proceedings of the National Academy of Sciences*, *114*(50), 13114–13119. https://doi.org/10.1073/pnas.1702143114

Clark, P. U. (2012). Ice Sheets in Transition. *Science*, *337*(6095), 656–658. https://doi.org/10.1126/science.1226335

Clark, Peter U., & Pollard, D. (1998). Origin of the Middle Pleistocene Transition by ice sheet erosion of regolith. *Paleoceanography*, *13*(1), 1–9. https://doi.org/10.1029/97PA02660

Continental shield | geology. (n.d.). Encyclopedia Britannica. Retrieved April 24, 2020, from https://www.britannica.com/science/continental-shield

Cook, C. P., van de Flierdt, T., Williams, T., Hemming, S. R., Iwai, M., Kobayashi, M., Jimenez-Espejo, F. J., Escutia, C., González, J. J., Khim, B.-K., McKay, R. M., Passchier, S., Bohaty, S. M., Riesselman, C. R., Tauxe, L., Sugisaki, S., Galindo, A. L., Patterson, M. O., Sangiorgi, F., … Yamane, M. (2013). Dynamic behaviour of the East Antarctic ice sheet during Pliocene warmth. *Nature Geoscience*, *6*(9), 765–769. https://doi.org/10.1038/ngeo1889

Corrigan, D, Van Rooyen, D., Morin, A., Houlé, M. G., & Bédard, M.-P. (2016). *Report of activities for the Core Zone and bounding orogens: Recent observations from the New Quebec Orogen in the Schefferville area, Quebec and Labrador, GEM-2 Hudson-Ungava Project* (No. 8127; p. 8127). https://doi.org/10.4095/299249

Corrigan, David, Wodicka, N., Mcfarlane, C., Lafrance, I., van Rooyen, D., Bandyayera, D., & Bilodeau, C. (2018). Lithotectonic Framework of the Core Zone, Southeastern Churchill Province, Canada. *Geoscience Canada*, *45*, 1–24. https://doi.org/10.12789/geocanj.2018.45.128

Corrigan et al. - 2016—Report of activities for the Core Zone and boundin.pdf. (n.d.).

Day, J. M. D., Brandon, A. D., & Walker, R. J. (2016). Highly Siderophile Elements in Earth, Mars, the Moon, and Asteroids. *Reviews in Mineralogy and Geochemistry*, *81*(1), 161–238. https://doi.org/10.2138/rmg.2016.81.04

Dutton, A., Carlson, A. E., Long, A. J., Milne, G. A., Clark, P. U., DeConto, R., Horton, B. P., Rahmstorf, S., & Raymo, M. E. (2015). Sea-level rise due to polar ice-sheet mass loss during past warm periods. *Science*, *349*(6244), aaa4019–aaa4019. https://doi.org/10.1126/science.aaa4019

Elderfield, H., Ferretti, P., Greaves, M., Crowhurst, S., McCave, I. N., Hodell, D., & Piotrowski, A. M. (2012). Evolution of Ocean Temperature and Ice Volume Through the Mid-Pleistocene Climate Transition. *Science*, *337*(6095), 704–709. https://doi.org/10.1126/science.1221294

Esser, B. K., & Turekian, K. K. (1993). Anthropogenic osmium in coastal deposits. *Environmental Science & Technology*, *27*(13), 2719–2724. https://doi.org/10.1021/es00049a010

Frank, M. (2002). Radiogenic isotopes: Tracers of past ocean circulation and erosional input. *Reviews of Geophysics*, *40*(1), 1001. https://doi.org/10.1029/2000RG000094

Hemming, S. R. (2004). Heinrich events: Massive late Pleistocene detritus layers of the North Atlantic and their global climate imprint. *Reviews of Geophysics*, *42*(1), RG1005. https://doi.org/10.1029/2003RG000128

Hodell, D. A., Channell, J. E. T., Curtis, J. H., Romero, O. E., & Röhl, U. (2008). Onset of "Hudson Strait" Heinrich events in the eastern North Atlantic at the end of the middle Pleistocene transition (~640 ka)?: PLEISTOCENE HEINRICH EVENTS. *Paleoceanography*, *23*(4), n/a-n/a. https://doi.org/10.1029/2008PA001591

John Marshall, R. Alan Plumb. (2008). *Atmosphere, ocean, and climate dynamics: An introductory text* (Vol. 45). http://choicereviews.org/review/10.5860/CHOICE.45-5595

Masson-Delmotte, V., Schulz, M., Abe-Ouchi, A., Beer, J., Ganopolski, A., Fidel, J., Rouco, G., Jansen, E., Lambeck, K., Luterbacher, J., Naish, T., Ramesh, R., Rojas, M., Shao, X., Anchukaitis, K., Arblaster, J., Bartlein, P. J., Benito, G., Clark, P., … Wanner, H. (n.d.). *Information from Paleoclimate Archives*. 82.

Mindat.org—Mines, Minerals and More. (n.d.). Retrieved April 24, 2020, from https://www.mindat.org/

Naafs, B. D. A., Hefter, J., & Stein, R. (2013). Millennial-scale ice rafting events and Hudson Strait Heinrich(-like) Events during the late Pliocene and Pleistocene: A review. *Quaternary Science Reviews*, *80*, 1–28. https://doi.org/10.1016/j.quascirev.2013.08.014

North America—Tectonic evolution. (n.d.). Encyclopedia Britannica. Retrieved April 24, 2020, from https://www.britannica.com/place/North-America

Nyman, K. H. M., & Ditlevsen, P. D. (2019). The middle Pleistocene transition by frequency locking and slow ramping of internal period. *Climate Dynamics*, *53*(5–6), 3023–3038. https://doi.org/10.1007/s00382-019-04679-3

Orthogneiss | geology. (n.d.). Encyclopedia Britannica. Retrieved April 24, 2020, from https://www.britannica.com/science/orthogneiss

Oxburgh, R., Pierson-Wickmann, A.-C., Reisberg, L., & Hemming, S. (2007). Climate-correlated variations in seawater 187Os/188Os over the past 200,000 yr: Evidence from the Cariaco Basin, Venezuela. *Earth and Planetary Science Letters*, *263*(3–4), 246–258. https://doi.org/10.1016/j.epsl.2007.08.033

Paquay, F. S., & Ravizza, G. (2012). Heterogeneous seawater 187Os/188Os during the Late Pleistocene glaciations. *Earth and Planetary Science Letters*, *349–350*, 126–138. https://doi.org/10.1016/j.epsl.2012.06.051

Peucker-Ehrenbrink, B., & Ravizza, G. (2000). The marine osmium isotope record. *Terra Nova*, *12*(5), 205–219. https://doi.org/10.1046/j.1365-3121.2000.00295.x

Peucker-Ehrenbrink, B., & Ravizza, G. (2012). Osmium Isotope Stratigraphy. In *The Geologic Time Scale* (pp. 145–166). Elsevier. https://doi.org/10.1016/B978-0-444-59425-9.00008-1

Peucker-Ehrenbrink, Bernhard, & Blum, J. D. (1998). Re-Os isotope systematics and weathering of Precambrian crustal rocks: Implications for the marine osmium isotope record. *Geochimica et Cosmochimica Acta*, *62*(19–20), 3193–3203. https://doi.org/10.1016/S0016-7037(98)00227-0

Ph. D., B. S., B. A., P. and M., Facebook, F., & Twitter, T. (n.d.). *What Quartzite Is and Where to Find This Rock*. ThoughtCo. Retrieved April 24, 2020, from https://www.thoughtco.com/quartzite-rock-geology-and-uses-4588608

Raymo, M. E., & Huybers, P. (2008). Unlocking the mysteries of the ice ages. *Nature*, *451*(7176), 284–285. https://doi.org/10.1038/nature06589

Roe, G. (n.d.). *In defense of Milankovitch*. 17.

Rooney, A. D., Selby, D., Lloyd, J. M., Roberts, D. H., Lückge, A., Sageman, B. B., & Prouty, N. G. (2016). Tracking millennial-scale Holocene glacial advance and retreat using osmium isotopes: Insights from the Greenland ice sheet. *Quaternary Science Reviews*, *138*, 49–61. https://doi.org/10.1016/j.quascirev.2016.02.021

Rotich, E. K., Handler, M. R., Naeher, S., Selby, D., Hollis, C. J., & Sykes, R. (2020). Re-Os geochronology and isotope systematics, and organic and sulfur geochemistry of the middle–late Paleocene Waipawa Formation, New Zealand: Insights into early Paleogene seawater Os isotope composition. *Chemical Geology*, *536*, 119473. https://doi.org/10.1016/j.chemgeo.2020.119473

ScienceDirect.com | Science, health and medical journals, full text articles and books. (n.d.). Retrieved April 24, 2020, from https://www.sciencedirect.com/

Shakun, J. D., Raymo, M. E., & Lea, D. W. (2016). An early Pleistocene Mg/Ca-δ^{18}O record from the Gulf of Mexico: Evaluating ice sheet size and pacing in the 41-kyr world: Early Pleistocene Meltwater Events. *Paleoceanography*, *31*(7), 1011–1027. https://doi.org/10.1002/2016PA002956

Shirey, S. B., & Walker, R. J. (1998). THE Re-Os ISOTOPE SYSTEM IN COSMOCHEMISTRY AND HIGH-TEMPERATURE GEOCHEMISTRY. *Annual Review of Earth and Planetary Sciences*, *26*(1), 423–500. https://doi.org/10.1146/annurev.earth.26.1.423

Stein, H., & Hannah, J. (2014). Rhenium–Osmium Geochronology: Sulfides, Shales, Oils, and Mantle. In W. J. Rink & J. Thompson (Eds.), *Encyclopedia of Scientific Dating Methods* (pp. 1–25). Springer Netherlands. https://doi.org/10.1007/978-94-007-6326-5_36-1

The southeastern Churchill Province: Synthesis of a Paleoproterozoic transpressional orogen | Request PDF. (n.d.). ResearchGate. http://dx.doi.org/10.1139/e02-004